
ALTRUISTIC RIDE SHARING: A FRAMEWORK FOR FAIR AND SUSTAINABLE URBAN MOBILITY VIA PEER-TO-PEER INCENTIVES

Divyanshu Singh

Dept. of CSIS and APPCAIR, BITS Pilani K K Birla Goa Campus, Goa, India
f20221129@goa.bits-pilani.ac.in

Ashman Mehra

School of Computer Science, Carnegie Mellon University, Pittsburgh, PA, USA
ashmanm@andrew.cmu.edu

Kavya Makwana

Dept. of CSIS and APPCAIR, BITS Pilani K K Birla Goa Campus, Goa, India
f20240634@goa.bits-pilani.ac.in

Snehanshu Saha

Dept. of CSIS and APPCAIR, BITS Pilani K K Birla Goa Campus, Goa, India
snehanshus@goa.bits-pilani.ac.in

Santonu Sarkar

Dept. of CSIS and APPCAIR, BITS Pilani K K Birla Goa Campus, Goa, India
santonus@goa.bits-pilani.ac.in

ABSTRACT

Urban mobility systems face persistent challenges of congestion, underutilized vehicles, and rising emissions driven by private point-to-point commuting. Although ride-sharing platforms exist, their profit-driven incentive structures often fail to align individual participation with broader community benefit. We introduce *Altruistic Ride Sharing* (ARS), a decentralized peer-to-peer mobility framework in which commuters alternate between driver and rider roles using *altruism points*, a non-monetary credit mechanism that rewards providing rides and discourages persistent free-riding. To enable scalable coordination among agents, ARS formulates ride-sharing as a multi-agent reinforcement learning problem and introduces *ORACLE* (One-Network Actor-Critic for Learning in Cooperative Environments), a shared-parameter learning architecture for decentralized rider selection. We evaluate ARS using real-world New York City Taxi and Limousine Commission (TLC) trajectory data under varying agent populations and behavioral dynamics. Across simulations, ARS reduces total travel distance and associated carbon emissions by approximately 20%, reduces urban traffic density by up to 30%, and doubles vehicle utilization relative to no-sharing baselines while maintaining balanced participation across agents. These results demonstrate that altruism-based incentives combined with decentralized learning can provide a scalable and equitable alternative to profit-driven ride-sharing systems.

Keywords Ride-Sharing · Multi-agent systems · Reinforcement Learning · Sustainable Urban Transportation · Social Incentives

I. Introduction

Urban mobility systems are increasingly strained as rapid urban population growth places growing pressure on road infrastructure, with point-to-point commuting remaining the dominant travel pattern. While conventional ride-sharing platforms such as UberPOOL and Lyft Line attempt to reduce inefficiencies through monetary incentives, their optimization objectives are primarily profit-driven rather than community-oriented. Carpooling adoption remains limited despite policy interventions, such as high-occupancy vehicle (HOV) lanes [18]. The primary reason for this is the lack of coordinated, community-driven solutions. A growing body of work has investigated ride-sharing driven by social incentives rather than financial ones. Ma and Hanrahan [12] analyzed peer-to-peer communities where shared needs foster more cooperative behavior. However, these efforts remained largely exploratory and lacked systematic integration with learning-based decision-making. Recent work has begun incorporating fairness considerations into ride-sharing systems. Vlachogiannis et al. [22] explored the design of monetary incentives using deep reinforcement learning for ridesharing, while Zhang et al. [28] focused on fairness with respect to race and income in travel demand forecasting. Zhou [29] employed Graph Attention Networks with Opinion Dynamics (OD-GAT) to improve prediction and reasoning of social relationships, enhancing service quality and ride-sharing safety. Zhou and Roncoli [31] introduce a joint pricing and matching framework that uses a fairness-aware discount function to maximize platform profit while ensuring equitable fares for passengers. Despite these advances, existing approaches largely remain focused on monetary incentives or predictive fairness, leaving the potential of community-driven cooperative ride-sharing largely unexplored. This paper introduces Altruistic Ride-Sharing (ARS), a decentralized, peer-to-peer mobility framework in which participants voluntarily alternate between being drivers (givers) and riders (takers). The key contributions of our work are summarized as follows:

- *Novel Concept:* The ARS model operates using the concept of *altruism points* as a mechanism for incentivizing cooperation and balanced participation instead of traditional monetary transactions. ARS is designed to minimize total travel distance, detours, and wait times while promoting fairness, sustainability, and system stability.
- *Role-Switching:* We introduce a probabilistic, altruism-driven role assignment model where agents dynamically switch between driver and rider roles, maintaining fairness and balance in the system (subsection II-D).
- *Population Modeling:* We design a biologically inspired birth–death–dropout process to simulate realistic participation, dropout, and re-entry behaviors. This improves system resilience and prevents persistent dominance of either drivers or riders.
- *Reinforcement Learning Integration:* We develop a multi-agent reinforcement learning framework based on the proposed ORACLE (One-Network Actor–Critic for Learning in Cooperative Environments) architecture. ORACLE employs parameter sharing and an attention-based critic to enable scalable decentralized ride-selection policies in dynamic urban environments (subsection II-F).
- *Continual Adaptation:* The ORACLE policy can operate as a human-in-the-loop recommendation system where drivers may accept, reject, or override suggested actions. These interactions generate off-policy experience that is incorporated into prioritized replay, allowing continual adaptation of the policy to evolving real-world behavior.
- *Model Stability:* The system dynamics implicitly promote fairness and long-term stability (paragraph III-A0c) in role distribution and altruism dynamics [18]. Stability here refers to the system’s ability to maintain a balanced driver–rider population while reintegrating agents who temporarily leave the platform and allowing them to rebuild their altruism scores.
- *Evaluation Framework:* Using real-world data from the New York City Taxi and Limousine Commission (TLC), we evaluate ARS across multiple metrics capturing efficiency, service quality, and fairness. The framework is benchmarked against several baselines including learning-based methods, optimization-based solvers, and a no-sharing scenario, demonstrating improvements in sustainability and cooperative participation.

The paper has been organized as follows. We present the relevant work in this area in Section V. Section II introduces the ARS framework, detailing its core components including the altruism score mechanism, the multi-agent reinforcement learning model, and the population. The simulation design, including the experimental setup, performance metrics, and baseline models, is described in Section III. We present and analyze the results of our experiments in Section IV. Finally, Section VI concludes the paper and discusses future research directions.

II. The Altruistic Ride Sharing Model

The Altruistic Ride-Sharing (ARS) framework models short-distance urban mobility as a decentralized peer-to-peer system in which participants dynamically alternate between two roles: *driver (giver)* and *rider (taker)*. Instead of

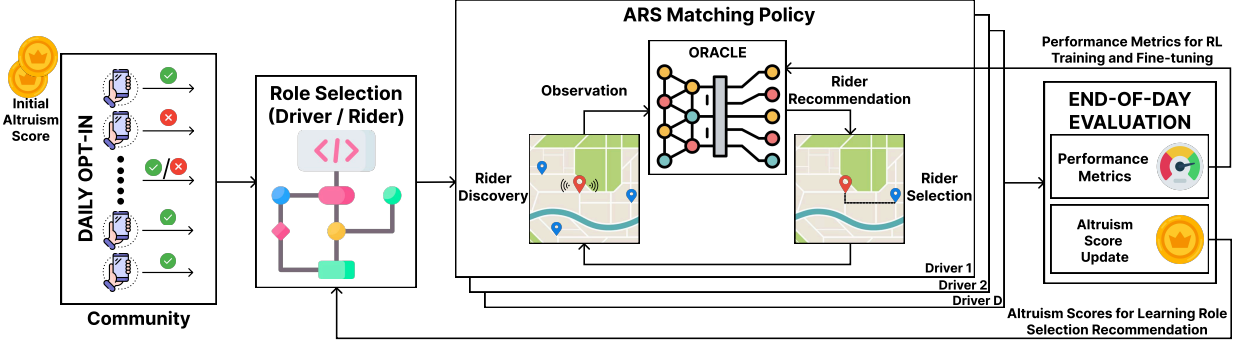


Fig. 1: Overview of the Altruistic Ride-Sharing (ARS) framework. Each day, community members join the system and receive role recommendations based on their altruism scores. Drivers use the ARS policy to select riders in real time using local observations. At the end of the day, system performance is evaluated and user scores are updated, creating a feedback loop that influences future role recommendations and policy learning.

financial transactions, participants exchange a virtual social currency called the *altruism score*, which reflects their contribution to the community.

Unlike conventional ride-hailing platforms where services can be repeatedly consumed through monetary payments, ARS operates as a closed-loop cooperative system. Altruism points must be earned by providing rides before they can be spent to request rides, encouraging reciprocal participation and discouraging persistent free-riding. This mechanism enables decentralized coordination while maintaining a balanced driver-rider population over time.

A. Core Concepts

1. **Agent.** An *agent* represents a commuter in the system. Let A denote the set of agents and $t \in \{1, \dots, T\}$ denote a simulation day. On day t , agents may act as drivers $D_t \subseteq A$, riders $R_t \subseteq A$, or remain inactive.
2. **Altruism Score.** Each agent a_i maintains an altruism score $s_i^t \in [0, 1]$ that reflects their contribution to the community. Altruism increases when providing rides and decreases when receiving rides.
3. **Popularticipation Dynamics.** Agents may dynamically join (*birth*), temporarily leave (*dropout*), or permanently exit (*death*) the system (subsection II-E).
4. **Detour Cost.** Detour cost measures the additional distance a driver travels to accommodate riders relative to their original direct route.

A comprehensive notation reference is provided in the supplementary material. Key variables are defined inline as they are introduced.

B. Optimization Objectives

The ARS system aims to balance individual travel efficiency with community-level benefits. We therefore define three objectives: minimizing driver detours, maximizing rider service coverage, and encouraging cooperative participation through altruism incentives.

Let $d_i(\cdot)$ denote the trip distance for agent a_i , where $d_i(\emptyset)$ is the direct solo trip distance without ride-sharing, and $d_i(\phi_i^t)$ is the total distance traveled by driver a_i on day t when serving a sequence of riders ϕ_i^t .

The objectives are defined as follows:

$$\text{Minimize } \mathbb{O}_1 : \sum_{t=1}^T \sum_{i=1}^{|D_t|} [d_i(\phi_i^t) - d_i(\emptyset)] \quad (1)$$

$$\text{Maximize } (\mathbb{O}_2, \mathbb{O}_3) : \sum_{t=1}^T \sum_{a_i \in R_t} \mathbb{I}(a_i \text{ gets ride on day } t) d_i(\emptyset), \quad \sum_{i=1}^{|A|} s_i^t \quad (2)$$

Objective \mathbb{O}_1 captures the additional distance incurred by drivers when serving riders, encouraging efficient ride-sharing routes. Objective \mathbb{O}_2 rewards serving riders with longer trips, reflecting the greater system-wide benefit

obtained when a shared ride replaces a longer solo trip. Objective \mathbb{O}_3 promotes sustained cooperative participation by maximizing the cumulative altruism scores across the agent population.

Rather than solving a strict multi-objective optimization problem, ARS approximates these objectives through the reward formulation used by the reinforcement learning policy (subsection II-F). The reward acts as a weighted scalarization of driver detour cost, rider trip benefit, and altruism incentives, guiding decentralized decision-making while implicitly balancing the objectives above.

The system operates under two practical constraints. First, drivers have a tolerance limit on detours to ensure ride-sharing remains feasible, restricting detours to at most 50% of the direct route. Second, each vehicle has a fixed seating capacity that limits the number of riders served per trip.

These objectives guide the decision-making of drivers within the ARS framework, while role assignment and altruism dynamics regulate participation across the agent population.

C. The Altruism Score (Virtual Currency)

The altruism score is a non-monetary incentive mechanism that regulates participation in the ARS community. Agents earn altruism by providing rides as drivers and spend it when requesting rides. Scores are bounded to the interval $[0, 1]$ to prevent long-term hoarding and encourage continued participation in both roles.

When a driver a_i provides a ride to rider a_j on day t , the driver's altruism increases according to

$$\Delta s_i^{t+1} = \alpha_s s_j^t \left(1 - \frac{d_i(\phi_i^t \parallel a_j) - d_i(\phi_i^t)}{\text{max_detour}} \right) \quad (3)$$

where $d_i(\phi_i^t \parallel a_j)$ denotes the route after adding rider a_j and max_detour represents the maximum allowable detour. Larger detours therefore yield smaller altruism gains.

The rider's altruism decreases proportionally to the benefit received, after which scores are clamped to remain within valid bounds:

$$\Delta s_j^{t+1} = -\beta_s \cdot \Delta s_i^{t+1}, \quad s_i^{t+1} = \max(0, \min(1, s_i^t + \Delta s_i^{t+1})) \quad (4)$$

This mechanism ensures that agents who repeatedly request rides must eventually contribute as drivers to replenish their altruism.

D. Daily Role Assignment (Probabilistic Switching)

At the beginning of each simulation day, agents are assigned roles based on their current altruism score. This mechanism promotes reciprocal participation while preventing persistent free-riding.

Agents with low altruism ($s_i^t \leq 0.2$) are required to act as drivers, ensuring that agents who have benefited from the system contribute back to the community. Agents with higher altruism ($s_i^t > 0.2$) select roles probabilistically according to their normalized altruism scores. A small exploration probability allows occasional random role selection to maintain behavioral diversity.

The resulting role assignment process is illustrated in Figure 2.

E. Population Dynamics and Network Adoption

Decentralized peer-to-peer mobility systems require sufficient participation to remain viable. To capture realistic community growth and retention, the ARS simulation incorporates a dynamic population model in which agents may enter, leave, and later rejoin the system. The overall process is illustrated in Figure 4.

Dropout Process. Agent retention is linked to the altruism economy. Agents with persistently low altruism scores have a higher probability of leaving the platform, reflecting reduced incentives when they cannot secure rides. Conversely, agents with higher altruism tend to remain active.

Birth Process. New agents join the system through a probabilistic adoption model capturing network effects and platform reputation:

$$P_{\text{birth}} = P_{\text{base}} \cdot F_{\text{phase}}(\rho) \cdot F_{\text{urgency}}(d) \cdot F_{\text{net}}(N_{\text{act}}) \cdot F_{\text{rep}}(\bar{s}) \quad (5)$$

where ρ denotes the current community adoption rate, N_{act} represents the number of active agents, and \bar{s} is the average altruism score of the population. The multiplier F_{phase} models adoption stages inspired by diffusion-of-innovation theory, while F_{net} and F_{rep} capture positive feedback from user density and system reputation.

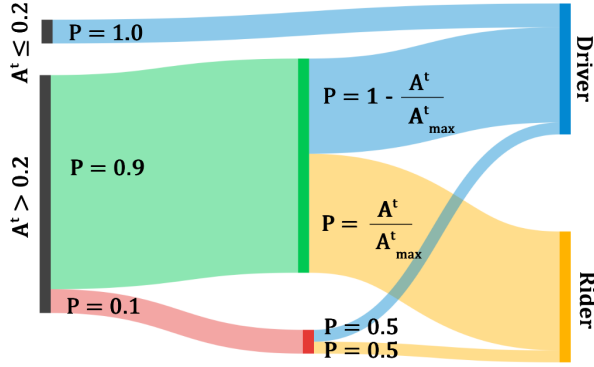


Fig. 2: Sankey diagram illustrating the probabilistic role assignment mechanism. Agents with low altruism (≤ 0.2) must act as drivers, while agents with higher altruism probabilistically choose between driver and rider roles based on their normalized scores.

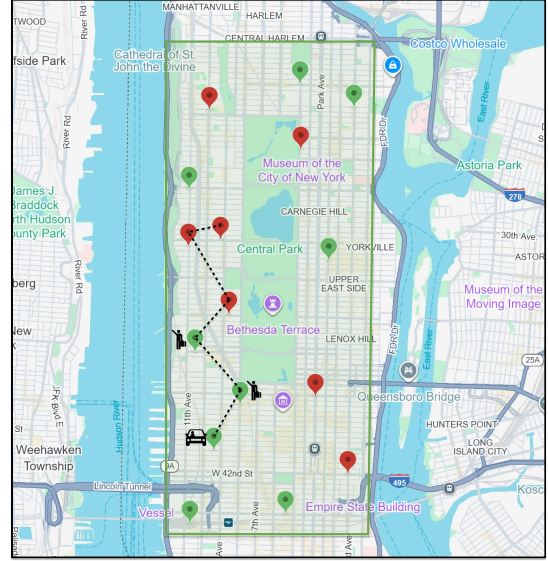


Fig. 3: The 15×15 grid overlay on the selected Manhattan corridor forming the simulation environment. Points represent trip origins and destinations sampled from the NYC TLC dataset.

To mitigate cold-start challenges, newly joining agents receive a small initialization bonus to their altruism score. This encourages early participation and helps the system reach a cooperative critical mass more rapidly.

Detailed definitions and mathematical formulations provided in the supplementary material.

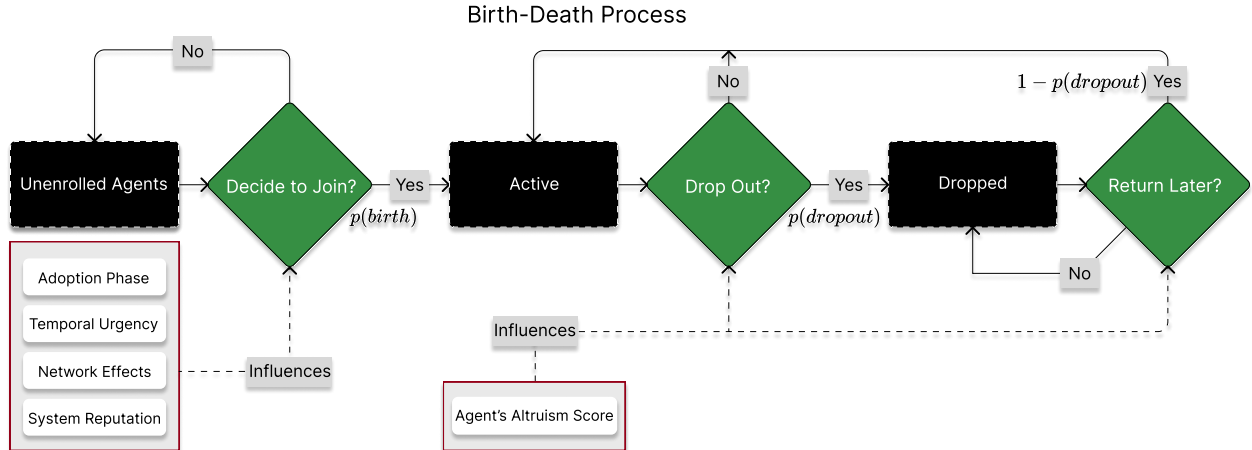


Fig. 4: Population dynamics in the ARS system. Agents may join the platform (birth), remain active, temporarily drop out, and later return. Adoption is influenced by network effects and system reputation, while dropout probability is linked to an agent's altruism score.

F. ORACLE: Shared-Parameter Learning Architecture

Ride-sharing environments involve large populations of agents making structurally similar decisions. Standard multi-agent reinforcement learning (MARL) methods such as MADDPG [11] or MAAC [7] maintain independent policy networks for each agent, causing the number of parameters and training instability to grow with population size. To support scalable learning in ARS, we introduce ORACLE (*One-Network Actor-Critic for Learning in Cooperative Environments*), a parameter-sharing MARL architecture designed for homogeneous agent populations.

Instead of learning separate policies for each agent, ORACLE trains a single shared actor network that is reused across all agents. Each agent conditions its decisions on its own observation while sharing the same policy

parameters. This allows knowledge learned by one agent to immediately benefit the entire population and enables the policy to generalize to varying numbers of active agents.

During centralized training, ORACLE employs an ego-conditioned attention-based critic to evaluate joint agent interactions. The critic processes the ego agent’s state together with contextual information from neighboring agents and the selected action, capturing coordination effects between drivers competing for riders in the local environment. The attention mechanism focuses on relevant agents while ignoring unrelated ones, improving learning stability in dense multi-agent settings.

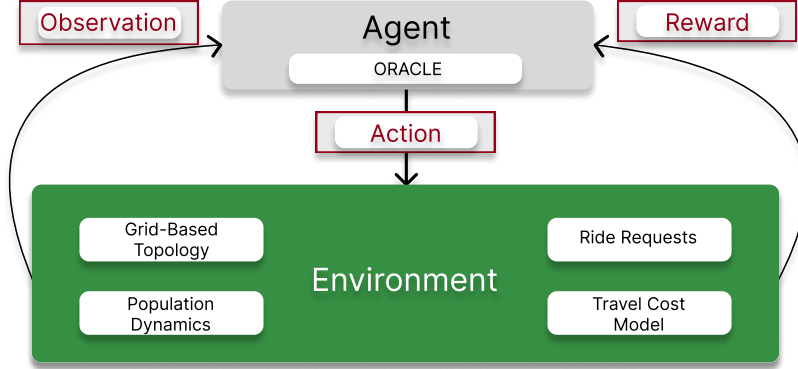


Fig. 5: Interaction loop of the ORACLE policy in the ARS system. Drivers observe local state information and select riders using the shared policy. Learning is guided by rewards that balance driver detour cost and altruism incentives.

The ORACLE policy operates using structured observations, discrete rider-selection actions, and a reward signal that balances efficiency and cooperative incentives.

a) Observation Space.: Each agent observes a structured state vector composed of three components:

- **Spatial coordinates:** The (x, y) position of the agent in the discrete grid environment.
- **Role identifier:** A binary indicator distinguishing drivers (1) from riders (0).
- **Local perception field:** A 5×5 observation grid centered on the agent that encodes nearby rider locations and local environmental context.

Together these components form a 28-dimensional observation vector.

b) Action Space.: Driver actions correspond to selecting riders from their local neighborhood. The action space is defined as $u \in \{0, 1, \dots, N\}$ where $u \in \{0, \dots, N - 1\}$ corresponds to selecting a specific rider for pickup and $u = N$ represents declining all available requests. To ensure feasibility, ORACLE employs *action masking*, which dynamically restricts available actions to riders visible within the local perception field. This prevents invalid assignments while maintaining computational efficiency.

c) Reward Mechanism.: To guide decentralized learning, ORACLE optimizes a scalar reward r_i that balances driver cost, rider benefit, and altruism incentives:

$$r_i = \tanh\left(\underbrace{\alpha_r \cdot d_j(\emptyset)}_{\text{rider trip saved}} - (1 - \alpha_r) \cdot \underbrace{\Delta d_i(a_j)}_{\text{driver detour cost}} + \underbrace{\Delta s_i^+}_{\text{altruism gain}}\right) \quad (6)$$

The first term rewards serving riders with longer trips, the second penalizes additional detour incurred by the driver, and the third captures altruism gains from the virtual currency mechanism. Together these terms encourage drivers to select riders that improve overall system efficiency while maintaining fair participation across the community.

G. Continual Adaptation via Human-in-the-Loop

In real-world deployment, the ORACLE policy can operate as a recommendation engine rather than a fully autonomous controller. Drivers may accept, delay, or override suggested rider selections based on factors that are difficult to model explicitly, such as personal schedules or perceived detour tolerance. These interactions generate

off-policy transitions that are stored in a prioritized experience replay (PER) buffer. Transitions with higher temporal-difference (TD) error are sampled more frequently during training, enabling the policy to focus on situations where model predictions diverge from observed behavior. This mechanism allows the ARS policy to continually adapt to evolving real-world driving patterns without requiring explicit exploration that could negatively affect service quality.

III. Altruistic Ride Sharing Simulation Design

This section describes the simulation environment used to evaluate the Altruistic Ride-Sharing (ARS) framework. The simulator integrates the ORACLE multi-agent reinforcement learning model with the population dynamics and altruism mechanisms introduced in section II. The goal of the simulation is to analyze how decentralized ride-selection policies influence system-level outcomes such as travel efficiency, congestion reduction, and cooperative participation.

A. Environment Modeling and Evaluation Metrics

The ARS environment is modeled as a multi-agent system operating on a discrete 15×15 grid representing an approximately 23 km^2 urban region derived from the New York City Taxi and Limousine Commission (TLC) Yellow Taxi dataset (January 2016).

Trips are filtered to a one-hour window (9:00–10:00 AM on January 2, 2016) within a Manhattan corridor and mapped to the nearest grid cells, reducing the continuous spatial space while preserving realistic travel patterns. Inter-cell travel distances are precomputed using the OpenStreetMap road network assuming an average speed of 25 km/h.

When a pickup is chosen, the driver’s route is updated and the resulting detour cost and altruism updates are applied. The environment evolves in discrete daily cycles consisting of role assignment, ride-selection interactions, route updates, and altruism score adjustments.

Population dynamics—including agent birth, dropout, and reintegration mechanisms described in subsection II-E, are also simulated to capture realistic variations in participation over time. Trips are sampled uniformly across distance ranges to ensure representative coverage of short and medium-distance urban travel.

Figure 3 illustrates the grid discretization and example trip trajectories used in the simulation.

This environment forms the basis for evaluating ARS under the metrics defined next.

a) System Efficiency Metrics:

- **Total Distance and Carbon Emissions.** Total distance traveled by all vehicles during the simulation. Carbon emissions are estimated as a linear function of total distance. Lower values indicate improved environmental efficiency.
- **Vehicle Utilization.** Measures the average occupancy of vehicles over time. Higher utilization indicates more efficient use of available vehicles through ride-sharing.
- **Road Traffic Density.** Measures the number of vehicles present in spatial grid cells of the city map during the simulation. Lower traffic density indicates reduced congestion.
- **Detour Factor.** Ratio of actual trip distance to the corresponding direct route.

b) Service Quality Metrics:

- **Average Trip Time.** Average travel time experienced by agents during a simulation day.
- **Rider Acceptance Rate.** Fraction of rider requests successfully matched with drivers. Higher acceptance rates indicate better service availability.

c) Fairness and Participation Metrics:

- **Benefit Distribution Analysis.** Evaluates inequality in ride-sharing benefits across agents using a 3D Lorenz surface and the Gini coefficient.

- **Reintegration Score.** Measures the system’s ability to reintegrate agents who temporarily leave the platform and later return. The score aggregates multiple aspects of user re-entry behavior:

$$REINT = \alpha R_{basic} + \beta R_{time} + \gamma R_{quick} + \delta R_{stable} \quad (7)$$

where R_{basic} is the overall return rate, R_{time} measures reintegration speed, R_{quick} captures short-term returns, and R_{stable} reflects long-term participation stability.

Detailed definitions and mathematical formulations of these metrics are provided in the supplementary material.

B. Baselines

We compare ARS against several learning-based, optimization-based, and system-level baselines to evaluate the effectiveness of the proposed framework. All learning-based baselines are trained using the same environment, reward structure, and observation space to ensure fair comparison.

a) Learning-Based Baselines:

- **MADDPG** [11]. A centralized-training decentralized-execution MARL algorithm where each agent maintains an independent actor–critic policy. In our experiments, each driver is modeled as an independent MADDPG agent trained within the same ARS environment and reward formulation.
- **MAAC** [7]. An actor–critic MARL method with an attention-based centralized critic. Agents operate using local observations while the critic selectively attends to relevant agents during training.

b) Optimization Baseline:

- **Particle Swarm Optimization (PSO)** [8]. PSO is used as a heuristic optimization baseline where each particle represents a rider–driver assignment configuration.

c) System Baseline:

- **No Ride Sharing.** Each agent travels directly to its destination without ride-sharing. This scenario provides a lower-bound reference for evaluating the impact of cooperative mobility.

IV. Performance Analysis and Results

We evaluate the Altruistic Ride-Sharing (ARS) framework through a series of simulations designed to analyze system-level efficiency, service quality, and cooperative participation. Experiments are conducted with agent populations of $N \in \{100, 150, 200\}$ to study system behavior under varying demand levels. For each configuration, 100 independent simulation runs are performed to ensure statistical robustness.

Agents are initialized with altruism scores drawn from two different distributions: a uniform distribution over $[0, 1]$ and a Gaussian distribution centered at 0.5 with bounded support in $[0, 1]$. This allows us to examine system dynamics under both evenly distributed and centrally concentrated cooperation levels.

We evaluate ARS under both fixed-population and dynamic population settings. In the fixed scenario, the number of agents remains constant throughout the simulation. In the dynamic scenario, agents may enter or leave the system according to the birth–death processes described in subsection II-E, enabling evaluation of system stability under evolving participation.

Across these experimental settings, we compare the ORACLE-based ARS model with learning-based baselines, optimization-based solvers, and a no-sharing scenario to quantify improvements in mobility efficiency, traffic reduction, and community participation.

A. ARS vs. No Sharing

We first compare the ARS framework against a baseline scenario in which agents travel independently without ride-sharing. Across the 100-day simulation horizon, ARS consistently reduces the total distance traveled by the community by approximately 20% across different agent populations and simulation settings (Figure 7). Because vehicle emissions are proportional to distance traveled, this reduction directly translates into a comparable decrease in estimated carbon emissions.

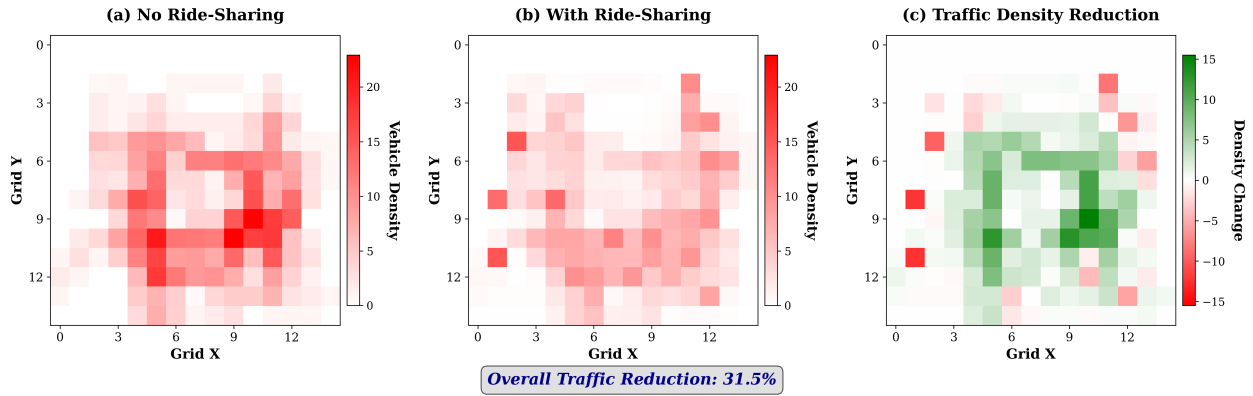


Fig. 6: Comparison of traffic density maps illustrating the reduction in urban congestion achieved by the ARS framework. The figure displays vehicle density for (a) the No Ride-Sharing baseline and (b) the With Ride-Sharing scenario. Subplot (c) visualizes the difference, quantifying a significant overall traffic reduction of 31.5%.

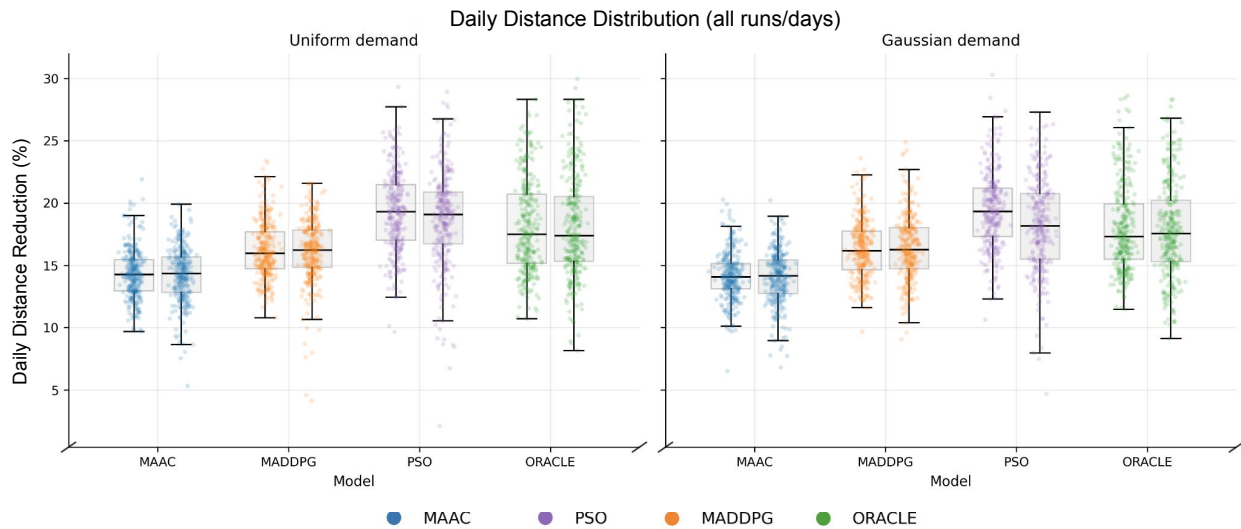


Fig. 7: Daily travel distance reduction across simulation runs under uniform (left) and Gaussian (right) demand distributions. PSO achieves the largest reductions through global optimization, while ORACLE closely competes with PSO while operating with decentralized decision-making.

In addition to environmental benefits, ARS substantially reduces road congestion. As shown in Figure 6, the number of vehicles occupying grid cells during peak periods decreases significantly under ARS, resulting in an overall traffic reduction of up to 31.5%. These results indicate that altruism-driven ride-sharing can improve transportation efficiency and reduce congestion without relying on monetary incentives. Beyond pure efficiency, the ARS framework was designed to be equitable and self-sustaining. Our results confirm its success in fostering a resilient and fair community and demonstrate its ability to recover users who drop out and maintain a stable, active user base over time. (Table II).

B. Architectural Advantages of ORACLE and Learning-Based Methods

Optimization-based approaches such as PSO can achieve strong performance on certain metrics under controlled conditions, particularly when rider requests and driver locations are available simultaneously for global assignment. However, these approaches treat ride matching as a static combinatorial problem and require repeatedly solving large optimization instances as the system state evolves.

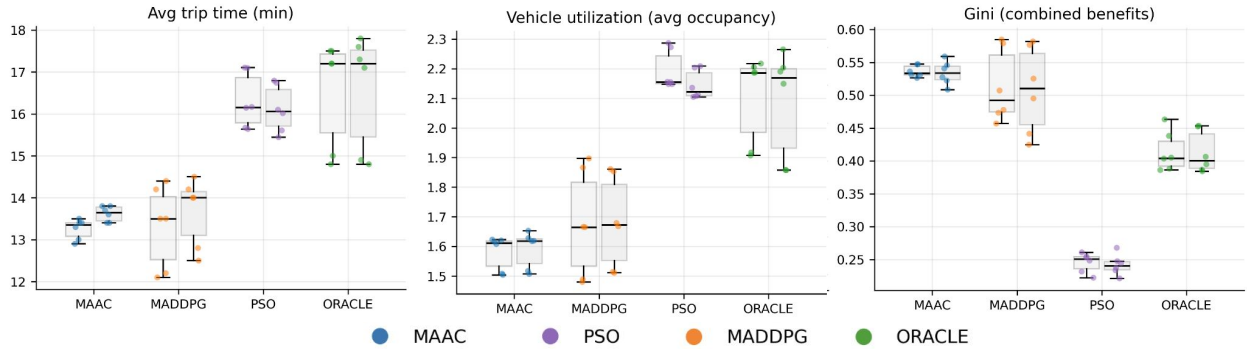


Fig. 8: Distribution of key performance metrics across ride-sharing methods. Box plots compare average trip time, vehicle utilization (average occupancy), and benefit inequality (Gini coefficient) for MAAC, MADDPG, PSO, and ORACLE. ORACLE achieves competitive utilization while maintaining lower inequality in benefit distribution compared to optimization-based approaches.

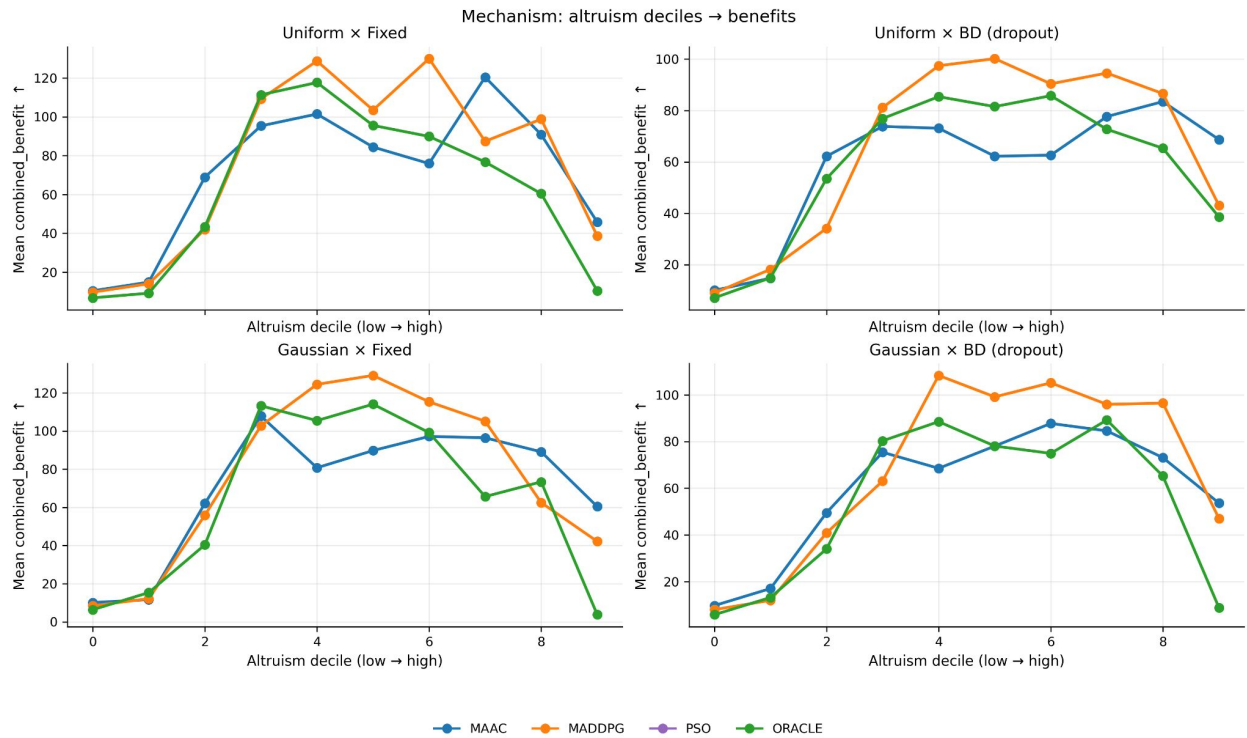


Fig. 9: Relationship between altruism score deciles and mean community benefit across different simulation settings. Results are shown for four initialization scenarios: Uniform and Gaussian altruism distributions with fixed populations and with birth–death dynamics. ORACLE maintains stable benefit allocation across altruism levels while avoiding the extreme concentration observed in some optimization-based assignments.

In real-world mobility systems, ride requests arrive asynchronously and drivers depart immediately after matching, making static batch assignment difficult to maintain in practice. Recomputing global assignments as new requests appear introduces significant computational overhead and may invalidate previously generated routes. In addition, evaluating candidate assignments in PSO requires solving small multi-rider routing problems (e.g., three- or four-rider TSP variants) for each driver, significantly increasing the computational cost of a single global optimization step compared to policy inference in learning-based approaches.

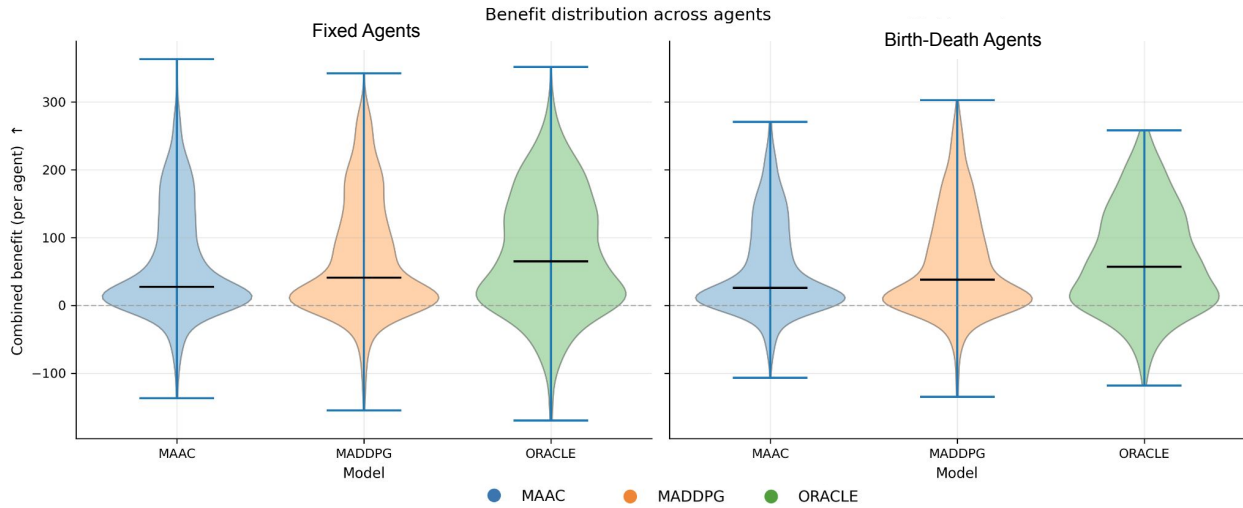


Fig. 10: Distribution of cumulative ride-sharing benefits across agents. Violin plots show the distribution of individual benefits for MAAC, MADDPG, and ORACLE under two population scenarios: fixed agents (left) and dynamic birth–death participation (right). ORACLE produces a more balanced benefit distribution while maintaining higher median community benefit, indicating improved fairness and sustained participation incentives.

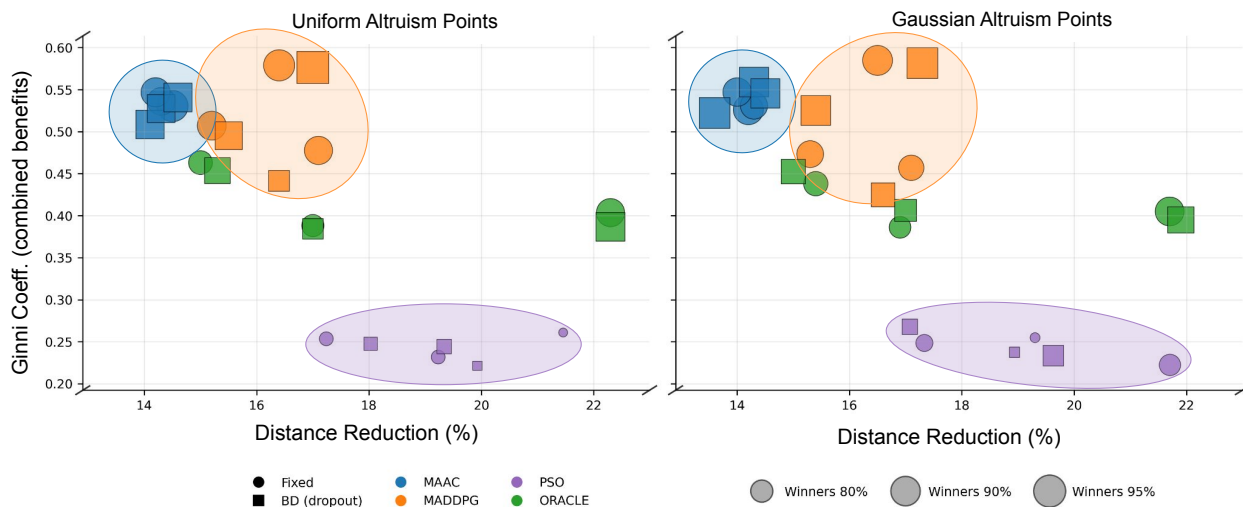


Fig. 11: Distance reduction vs. benefit inequality (Gini; lower is fairer) under uniform (left) and Gaussian (right) altruism initialization. ORACLE achieves competitive distance reduction while maintaining lower inequality than other learning-based methods.

Learning-based methods instead operate in a sequential decision-making setting where agents act based on locally observable information. This allows the system to process new ride requests incrementally while maintaining stable assignments over time.

This sequential decision structure also enables human-in-the-loop operation. Drivers may override recommended matches (e.g., rejecting or selecting a different rider), and the resulting transitions are incorporated into the prioritized experience replay buffer during training. As summarized in Table I, this makes human override support native to ORACLE. In contrast, global optimization approaches would require recomputing the full assignment when deviations occur, while MARL architectures such as MADDPG and MAAC rely on separate per-agent policies, making it difficult to consistently incorporate override behavior into a shared learning process.

Within this class of approaches, ORACLE introduces additional architectural advantages over standard multi-agent reinforcement learning methods such as MADDPG and MAAC. Rather than maintaining separate actor and critic

TABLE I: DEPLOYMENT-ORIENTED COMPARISON OF OPTIMIZATION AND LEARNING APPROACHES.

Deployment Dimension	PSO	MADDPG / MAAC	ORACLE
Information requirement	Static batch	Local obs.	Local obs.
Computational latency	~100× slower	~5× slower	Fast
Live requests	No	Yes	Yes
Human override	Infeasible	Difficult	Native
Acceptance rate (batch)	Highest	Moderate	Moderate
Stability (Reintegration)	Not modeled	Moderate (78.20)	High (89.40)

Latency measured relative to ORACLE inference time.

TABLE II: SUMMARY OF REINTEGRATION METRICS - ORACLE

Metric	Value
Final Score ↑	89.40
Basic Rate ↑	0.9888
Time-Weighted Rate ↑	0.8039
Quick Return Rate ↑	0.9887
Stability Score ↑	0.8316
Avg. Return Time (d) ↓	1.10

TABLE III: AVG. VEHICLE UTILIZATION AND DETOUR FACTOR METRICS

Method	Utilization ↑	Detour ↓
ORACLE	2.10	1.27
MADDPG	1.68	1.14
PSO	2.17	1.53
MAAC	1.59	1.19

networks for each agent, ORACLE uses a single shared network that evaluates the joint state from the perspective of an ego agent using an attention-based critic.

This shared-network formulation reduces parameter complexity, improves training stability, and enables continual adaptation through real-world interaction. Empirically, ORACLE achieves stronger performance across efficiency, fairness, and utilization metrics while remaining computationally more efficient than both optimization-based baselines and existing learning-based architectures.

a) Community Fairness and System Resilience.: Beyond pure efficiency, the ARS framework was designed to be equitable and self-sustaining. Our results confirm its success in fostering a resilient and fair community. The model’s high Reintegration Score of *89.40* and Stability Score of *0.8316* demonstrate its ability to recover users who drop out and maintain a stable, active user base over time (Table II).

b) Closed Economy Design.: ARS intentionally operates as a closed incentive economy in which altruism points can only be earned through providing rides and spent when receiving rides. No external mechanisms such as point purchasing or membership tiers are allowed. This restriction preserves the interpretability of altruism scores as a measure of community contribution and ensures that role assignment remains tied to actual participation. Allowing external injection of altruism points would break this signal and destabilize the driver–rider equilibrium. A detailed analysis of these failure modes is provided in the supplementary material.

V. Related Work

Research on ride-sharing has evolved across optimization methods, reinforcement learning frameworks, and decentralized coordination mechanisms. Wen et al. [26] review machine learning approaches for ride-hailing and categorize planning strategies into two key tasks: matching (assigning vehicles to riders) and repositioning (relocating vehicles to meet anticipated demand), further distinguishing between centralized collective planning and distributed agent-based decision-making. Broader surveys by Qin et al. [16] examine reinforcement learning applications in ride-sharing, while recent studies explore hybrid transit systems [9] and pooled routing with passenger transfers [23], highlighting growing interest in multi-modal and socially responsible transport systems.

Optimization-Based Ride-Sharing. Traditional ride-sharing research largely focuses on centralized optimization for system-wide efficiency. Alonso-Mora et al. [4] introduced a real-time high-capacity ride-pooling algorithm capable of handling large-scale urban demand. Zhou and Roncoli [31] extended this paradigm with a joint pricing and matching framework incorporating fairness-aware discounts. To address scalability, distributed approaches have also been explored. Masoud and Jayakrishnan [13] proposed heuristic-based peer-to-peer matching, while Wang et al. [24] investigated privacy-preserving decentralized ride-sharing. CARE-Share [1] further explored fully distributed

multi-objective optimization using ant colony techniques. However, most optimization-based systems rely on static assumptions and lack mechanisms to adapt to dynamic user behaviors or fairness considerations.

Reinforcement Learning in Ride-Sharing. Reinforcement learning has become a natural framework for dynamic ride-matching. Tang et al. [20] proposed a deep value-network dispatcher, while DeliverAI [14, 15] extended RL-based routing to logistics systems. Deep reinforcement learning further enables scalable decision making, with frameworks such as DQN [6] inspiring applications like DeepPool [2] and its distributed extensions [5, 19]. Other works improve coordination using mean-field approximations [17], distribution matching [27], hierarchical MARL [30], transfer learning [3], and attention mechanisms [10]. Wei et al. [25] introduced lookahead-based RL for real-time ride matching. Despite these advances, most RL systems remain economically driven, optimizing revenue, latency, or fleet utilization rather than community-driven cooperation.

VI. Conclusion and Future Work

This paper presented Altruistic Ride-Sharing (ARS), an innovative framework designed to enhance short-distance urban mobility through community involvement. Distinct from profit-based ride-sharing models, ARS replaces financial incentives with altruism points, a virtual currency improving cooperation and mutual support. Employing multi-agent reinforcement learning (ORACLE), ARS offers a fair, scalable, and sustainable resolution to urban transport inefficiencies. Analysis utilizing real New York City taxi data reveals that ARS substantially cuts travel distances, reduces carbon emissions and traffic congestion, while enhancing vehicle utilization and service equity. Through altruism-based incentives, the system achieves equilibrium between drivers and riders, positioning ARS as a practical alternative to profit-driven urban mobility.

To improve system robustness, future work must incorporate more realistic and non-cooperative behaviors, such as modeling dishonest participants (e.g., no-shows, deliberate dropouts). Future work should also explore practical trust and safety mechanisms for real-world deployment, such as user verification and reputation-based accountability systems. To counter the reality that “real users may be strategic and malicious”, this requires developing a better game-theoretic model (e.g., one based on incomplete information or adversarial search) to analyze and mitigate non-cooperative strategies. In addition to the current grid structure, future works could also explore using dynamic road graph topology (e.g., a high-performance, *GraphHopper*-based structure).

References

- [1] et. al, M.: CARE-Share: A Cooperative and Adaptive Strategy for Distributed Taxi Ride Sharing . <https://doi.org/10.1109/TITS.2021.3066439>
- [2] Al-Abbasi, A.O., Ghosh, A., Aggarwal, V.: DeepPool: Distributed Model-Free Algorithm for Ride-Sharing Using Deep Reinforcement Learning. *IEEE Transactions on Intelligent Transportation Systems* **20**(12), 4714–4727 (Dec 2019). <https://doi.org/10.1109/TITS.2019.2931830>, <https://ieeexplore.ieee.org/document/8793143/>
- [3] Alberto Castagna, I.D.: Multi-Agent Transfer Learning in Reinforcement Learning-Based Ride-Sharing Systems. In: *AAAI* (2022)
- [4] Alonso-Mora, J., Samaranayake, S., Wallar, A., Frazzoli, E., Rus, D.: On-demand high-capacity ride-sharing via dynamic trip-vehicle assignment. *Proceedings of the National Academy of Sciences* **114**(3), 462–467 (2017)
- [5] Haliem, M., Mani, G., Aggarwal, V., Bhargava, B.: A Distributed Model-Free Ride-Sharing Approach for Joint Matching, Pricing, and Dispatching Using Deep Reinforcement Learning. *IEEE Transactions on Intelligent Transportation Systems* **22**(12), 7931–7942 (Dec 2021). <https://doi.org/10.1109/TITS.2021.3096537>, <https://ieeexplore.ieee.org/document/9507388/>
- [6] van Hasselt, H., Guez, A., Silver, D.: Deep reinforcement learning with double q-learning (2015), <https://arxiv.org/abs/1509.06461>
- [7] Iqbal, S., Sha, F.: Actor-attention-critic for multi-agent reinforcement learning (2019), <https://arxiv.org/abs/1810.02912>
- [8] Kennedy, J., Eberhart, R.: Particle swarm optimization. In: *Proceedings of ICNN'95 - International Conference on Neural Networks*. vol. 4, pp. 1942–1948 vol.4 (1995). <https://doi.org/10.1109/ICNN.1995.488968>
- [9] Kumar, P., Khani, A.: An algorithm for integrating peer-to-peer ridesharing and schedule-based transit system for first mile/last mile access. *Transportation Research Part C: Emerging Technologies* **122**, 102891 (Jan 2021). <https://doi.org/10.1016/j.trc.2020.102891>, <https://linkinghub.elsevier.com/retrieve/pii/S0968090X20307919>
- [10] Li, X., Wang, J., Xu, Q., Liu, Y.: Efficient Ridesharing Dispatch Using Multi-Agent Reinforcement Learning. *IEEE Transactions on Intelligent Transportation Systems* (2021)
- [11] Lowe, R., Wu, Y., Tamar, A., Harb, J., Abbeel, P., Mordatch, I.: Multi-agent actor-critic for mixed cooperative-competitive environments. In: *Advances in Neural Information Processing Systems (NeurIPS)*. pp. 6379–6390

- (2017)
- [12] Ma, N.F., Hanrahan, B.V.: Unpacking Sharing in the Peer-to-Peer Economy: The Impact of Shared Needs and Backgrounds on Ride-Sharing. *Proceedings of the ACM on Human-Computer Interaction* **4**(CSCW1), 1–19 (May 2020). <https://doi.org/10.1145/3392865>, <https://dl.acm.org/doi/10.1145/3392865>
 - [13] Masoud, N., Jayakrishnan, R.: A real-time algorithm to solve the peer-to-peer ride-matching problem in a flexible ridesharing system. *Transportation Research Part B: Methodological* **106**, 218–236 (Dec 2017). <https://doi.org/10.1016/j.trb.2017.10.006>, <https://linkinghub.elsevier.com/retrieve/pii/S0191261517301169>
 - [14] Mehra, A., Saha, S., Raychoudhury, V., Mathur, A.: DeliverAI: Reinforcement Learning Based Distributed Path-Sharing Network for Food Deliveries. In: 2024 International Joint Conference on Neural Networks (IJCNN). pp. 1–9 (Jun 2024). <https://doi.org/10.1109/IJCNN60899.2024.10651403>, <https://ieeexplore.ieee.org/abstract/document/10651403>, iSSN: 2161-4407
 - [15] Mehra, A., Singh, D., Raychoudhury, V., Mathur, A., Saha, S.: Last Mile: A Novel, Hotspot-Based Distributed Path-Sharing Network for Food Deliveries. *IEEE Transactions on Intelligent Transportation Systems* **25**(12), 20574–20587 (Dec 2024). <https://doi.org/10.1109/TITS.2024.3465217>, <https://ieeexplore.ieee.org/abstract/document/10705350>
 - [16] Qin, Z.T., Zhu, H., Ye, J.: Reinforcement learning for ridesharing: An extended survey. *Transportation Research Part C: Emerging Technologies* **144**, 103852 (Nov 2022). <https://doi.org/10.1016/j.trc.2022.103852>, <https://linkinghub.elsevier.com/retrieve/pii/S0968090X22002716>
 - [17] Qin, Z., Zhang, J., Ye, S., Zheng, Z., Xu, H.: Efficient Ridesharing Order Dispatching with Mean Field Multi-Agent Reinforcement Learning. In: *Proceedings of the AAAI Conference on Artificial Intelligence*. vol. 34, pp. 723–730 (2020)
 - [18] Shoham, Y., Leyton-Brown, K.: *Multiagent Systems: Algorithmic, Game-Theoretic, and Logical Foundations*. Cambridge University Press (2008)
 - [19] Singh, A., Al-Abbasi, A.O., Aggarwal, V.: A Distributed Model-Free Algorithm for Multi-Hop Ride-Sharing Using Deep Reinforcement Learning. *IEEE Transactions on Intelligent Transportation Systems* **23**(7), 8595–8605 (Jul 2022). <https://doi.org/10.1109/TITS.2021.3083740>, <https://ieeexplore.ieee.org/document/9477304/>
 - [20] Tang, X., Qin, Z., Zhang, F., Wang, Z., Xu, Z., Ma, Y., Zhu, H., Ye, J.: A deep value-network based approach for multi-driver order dispatching (2021), <https://arxiv.org/abs/2106.04493>
 - [21] Tilbury, C.R., Christianos, F., Albrecht, S.V.: Revisiting the gumbel-softmax in maddpg (2023), <https://arxiv.org/abs/2302.11793>
 - [22] Vlachogiannis, D.M., Wei, H., Moura, S., Macfarlane, J.: Humanlight: Incentivizing ridesharing via human-centric deep reinforcement learning in traffic signal control (2023), <https://arxiv.org/abs/2304.03697>
 - [23] Wang, D., Wang, Q., Yin, Y., Cheng, T.: Optimization of ride-sharing with passenger transfer via deep reinforcement learning. *Transportation Research Part E: Logistics and Transportation Review* **172**, 103080 (Apr 2023). <https://doi.org/10.1016/j.tre.2023.103080>, <https://linkinghub.elsevier.com/retrieve/pii/S1366554523000686>
 - [24] Wang, Q., Zhao, Y., Chen, X., Zhang, Y., Luo, J.: pdride: Privacy-preserving distributed on-line ride-hailing. *IEEE Transactions on Intelligent Transportation Systems* **24**(9), 9588–9600 (2023). <https://doi.org/10.1109/TITS.2022.3174598>
 - [25] Wei, H., Wang, X., Zhang, R., Zhang, Z.: A reinforcement learning and prediction-based lookahead framework for real-time ride matching. *IEEE Transactions on Intelligent Transportation Systems* **25**(8), 7841–7853 (2024). <https://doi.org/10.1109/TITS.2023.3351120>
 - [26] Wen, D., Li, Y., Lau, F.C.M.: A survey of machine learning-based ride-hailing planning. *IEEE Transactions on Intelligent Transportation Systems* **25**(6), 4734–4753 (2024). <https://doi.org/10.1109/TITS.2023.3345174>
 - [27] Zhang, C., Wang, L., Wang, J., Xu, H.: Multi-agent reinforcement learning for order-dispatching via order-vehicle distribution matching. *arXiv preprint arXiv:1905.01855* (2019)
 - [28] Zhang, X., Ke, Q., Zhao, X.: Travel demand forecasting: A fair ai approach. *IEEE Transactions on Intelligent Transportation Systems* **25**(10), 14611–14627 (2024). <https://doi.org/10.1109/TITS.2024.3395061>
 - [29] Zhou, Q.: An intelligent ride-sharing recommendation method based on deep learning and multi-objective optimization. *IEEE Transactions on Intelligent Transportation Systems* **26**(1), 711–723 (2025). <https://doi.org/10.1109/TITS.2024.3485985>
 - [30] Zhou, Y., Wang, H., Wang, Y., Xu, H., Liu, Z., Yu, Y.: Multi-agent mix hierarchical deep reinforcement learning for large-scale fleet management. In: *Proceedings of the AAAI Conference on Artificial Intelligence*. vol. 34, pp. 723–730 (2020)
 - [31] Zhou, Z., Roncoli, C.: A fairness-aware joint pricing and matching framework for dynamic ridesharing. In: 2023 8th International Conference on Models and Technologies for Intelligent Transportation Systems (MT-ITS). pp. 1–6 (2023). <https://doi.org/10.1109/MT-ITS56129.2023.10241664>

Appendix A Notation and Symbols

Tables V and IV collect all symbols used in the paper. Environment and problem-level symbols appear in Table V; learning and population-model parameters appear in Table IV.

TABLE IV: MODEL AND TRAINING PARAMETERS

Symbol	Meaning
<i>ORACLE training parameters</i>	
π_θ	Shared actor network (parameters θ)
Q_ϕ	Shared ego-conditioned attention critic (parameters ϕ)
α_π	Actor learning rate
α_Q	Critic learning rate
γ	Discount factor
τ	Soft (Polyak) target-network update rate
λ	Actor weight regularisation coefficient
\mathcal{E}	Exploration strategy (ϵ -greedy, TAGS, or GST)
\mathcal{D}	Prioritised experience replay buffer
$\alpha_{\mathcal{D}}, \beta_{\mathcal{D}}$	PER prioritisation exponent and importance-sampling exponent
<i>Reward shaping</i>	
α_r	Trade-off weight between rider benefit and driver detour cost in the reward
α_s, β_s	Driver and rider altruism score scaling factors
<i>Population dynamics (birth/death)</i>	
α_{bd}	Base dropout probability when $s_i^d \approx 0$
β_{bd}	Exponential decay rate for low-altruism agents
γ_{bd}	Base dropout value for high-altruism agents
δ_{bd}	Linear decay range above altruism threshold s_{th}^d
s_{th}^d	Altruism threshold separating exponential and linear dropout regimes
$P_{dropout}$	Dropout probability (function of s_i^d)
P_{birth}	Birth probability for unenrolled agents
<i>Reintegration score</i>	
$\alpha, \beta, \gamma, \delta$	Weighting factors for the four reintegration components
λ_{re}	Time-decay parameter for time-weighted return rate
τ_{re}	Quick-return threshold (number of days)

TABLE V: ENVIRONMENT AND PROBLEM VARIABLES

Symbol	Meaning
N	Total number of agents
D	Total simulation days, $d \in \{1, \dots, D\}$
\mathcal{A}	Set of all agents, $\mathcal{A} = \{a_1, \dots, a_N\}$
$\mathcal{A}_{\text{active}}$	Set of active agents on a given day
\mathcal{D}_d	Set of drivers on day d , $\mathcal{D}_d \subseteq \mathcal{A}_{\text{active}}$
\mathcal{R}_d	Set of riders on day d , $\mathcal{R}_d \subseteq \mathcal{A}_{\text{active}}$
\mathbf{M}	Role assignment map; $\mathbf{M}_i \in \{\text{driver, rider}\}$
s_i^d	Altruism score of agent a_i at the end of day d , $s_i^d \in [0, 1]$
s_{\max}^d	Maximum altruism score on day d , $s_{\max}^d = \max_i s_i^d$
Φ^d	Set of all rider pick-up permutations on day d , $\Phi^d = \bigcup_{k=0}^{ \mathcal{R}_d } \text{Perm}_k(\mathcal{R}_d)$
ϕ_i^d	Ordered rider pick-up sequence for driver a_i on day d , $\phi_i^d \in \Phi^d$
l_i	Vehicle capacity of driver a_i , $l_i \in \{1, \dots, 4\}$
$d_i(\cdot)$	Trip distance function for a_i ; $d_i : \Phi^d \rightarrow \mathbb{R}$; $d_i(\emptyset) = \text{solo trip}$
s_i	Observation of agent a_i at the current time-step
u_i	Action of a_i ; $u_i \in \{0, \dots, N\}$ $u_i = j$: pick up a_j ; $u_i = N$: no pick-up (no-op)
r_i	Scalar reward received by a_i from the environment
\mathbf{m}_i	Binary valid-action mask for agent a_i
$\rho(d)$	Community adoption rate at day d : fraction of the population that has joined

Appendix B

Closed Economy Design

The altruism score update in Equations 8 - 10 defines a **closed economy**: points enter the system only when a ride is given, and leave only when a ride is received. No external source of altruism exists. This section explains why that constraint is load-bearing, not incidental. Two natural extensions, (a) letting agents purchase points, and (b) granting premium members better service each collapse a different pillar of the system. We show this by tracing the failure through the existing equations.

A. What the Closed Economy Currently Guarantees

Recall the altruism update from the ARS model. When driver a_i gives a ride to rider a_j , the driver's score increases by:

$$\Delta s_i^{t+1} = \alpha_s s_j^t \left(1 - \frac{d_i(\phi_i^t \| a_j) - d_i(\phi_i^t)}{\text{max_detour}} \right) \quad (8)$$

and the rider's score decreases by:

$$\Delta s_j^{t+1} = -\beta_s \cdot \Delta s_i^{t+1} \quad (9)$$

Scores are clamped after updates to remain within valid bounds:

$$s_i^{t+1} = \max(0, \min(1, s_i^t + \Delta s_i^{t+1})) \quad (10)$$

Three properties follow directly from this structure.

(P1) Score reflects contribution. s_i^t is a sufficient statistic for agent a_i 's net contribution history. A high score means the agent has driven more than they have ridden, net of detour costs. There is no other way to accumulate a high score.

(P2) Role assignment is incorruptible. The role-switching rule in Section 3.5 assigns driver obligations to agents with $s_i^t \leq 0.2$. Because score is contribution-derived, this rule assigns driving to agents who have not contributed enough — exactly the right agents.

(P3) The equilibrium constraint holds. Equation 8 requires $|D_t|/|R_t| \in [L, H]$ with $L > 1$. This is sustained because low-scoring agents are pushed into the driver role, maintaining a sufficient driver supply.

The two extensions below each destroy one or more of these properties.

B. Extension 1: Purchasable Altruism Points

Suppose agents may purchase additional altruism points at price $p > 0$ per unit. The score update in Equation 10 becomes:

$$s_i^{t+1} = \text{clip}(s_i^t + \Delta s_i^{t+1} + \lambda_i^t, 0, 1) \quad (11)$$

where $\lambda_i^t \geq 0$ is the quantity purchased by agent a_i on day t . Compare (A) with Eq. 10, whereas (A) can be written alternatively as $s_i^{t+1} = \max(0, \min(1, s_i^t + \Delta s_i^{t+1} + \lambda_i^t))$. The only addition is the λ_i^t term inside i.e. the purchased points. The 0, 1 are just the lower and upper bounds of the clamp.

a) P1 breaks immediately.: With $\lambda_i^t > 0$, a high score no longer implies contribution. It could reflect driving history, or it could reflect financial expenditure. The system cannot tell them apart.

b) P2 breaks as a consequence.: The role-switching rule assigns driver obligations based on $s_i^t \leq 0.2$. Under Equation (A), any agent willing to pay can keep $s_i^t > 0.2$ indefinitely, regardless of their actual contribution. The rule now assigns driving only to agents who are both low-contributors *and* unwilling to pay — a much smaller set than intended.

c) P3 breaks as a consequence.: Let $\mathcal{B}^t \subseteq A$ denote the set of agents who purchase points on day t . As rational self-interest predicts \mathcal{B}^t to grow (purchasing is cheaper than driving for sufficiently wealthy agents), the driver-rider ratio shifts toward:

$$\frac{|D_t|}{|R_t|} \rightarrow \frac{N - |\mathcal{B}^t|}{|\mathcal{B}^t|} \quad (12)$$

As $|\mathcal{B}^t|$ grows, the driver supply shrinks. A small pool of genuinely altruistic drivers ends up serving a large pool of paying riders. This is precisely the extractive dynamic that commercial platforms already exhibit. The closed economy was designed to prevent it.

d) Summary.: Purchasable points corrupt the signal value of s_i^t , disable the free-rider detection mechanism in Section 3.5 of the main paper, and undermine the equilibrium constraint in Equation 16. All three failures follow from the single change in Equation (A).

Remark 1. $\lambda_i^t \geq 0$ is the quantity purchased by agent a_i on day t at price $p > 0$ per unit, determined entirely by the agent’s rational self-interest rather than any system parameter. The score update under a purchasable regime then becomes:

$$s_i^{t+1} = \max(0, \min(1, s_i^t + \Delta s_i^{t+1} + \lambda_i^t)) \quad (13)$$

Note that λ_i^t is not a hyperparameter set by the system designer. It is a *decision variable* controlled entirely by the agent. Given a purchase price $p > 0$, a rational agent will always buy exactly enough points to stay above the rider eligibility threshold $s = 0.2$, and no more. Equation 13 makes this precise: if an agent’s score after the day’s natural update $s_i^t + \Delta s_i^{t+1}$ already exceeds 0.2, they purchase nothing ($\lambda_i^t = 0$); if it falls below, they purchase precisely the shortfall. This purchasing rule requires no assumption about agent wealth or utility functions beyond rationality. Any agent who prefers riding to driving will adopt it whenever p is finite. The collapse of the driver pool follows directly: since λ_i^t is always sufficient to maintain rider eligibility, no rational agent ever needs to drive unless they choose to, and the equilibrium constraint $|D_t|/|R_t| \geq L > 1$ can no longer be guaranteed by the altruism mechanism alone. *The driver pool collapse is now a logical consequence of the purchasing rule, not just an empirical claim.*

C. Extension 2: Premium Membership

Suppose a tiered membership model grants premium subscribers priority in rider matching. Let $\mathcal{P}^t \subseteq A$ denote premium agents, and let $\mu > 1$ be the priority multiplier applied to their selection probability. The MARL reward

in Equation 6 is unchanged, but the effective selection probability of a premium rider $a_j \in \mathcal{P}^t$ relative to a standard rider $a_k \notin \mathcal{P}^t$ with equal altruism score becomes:

$$\frac{P(\text{select } a_j)}{P(\text{select } a_k)} = \mu \cdot \frac{s_j^t}{s_k^t} = \mu \quad \text{when } s_j^t = s_k^t \quad (14)$$

The multiplier μ is independent of contribution history. A premium agent with $s_j^t = 0.21$ receives μ times the matching probability of a high-contributing standard agent with $s_k^t = 0.90$. Payment overrides contribution.

a) Fairness breaks.: The Benefit Distribution Analysis measures inequality using Gini coefficients over the agent population. In the closed economy, the Benefit Gini for distance savings is already ~ 0.35 . This implies that moderate inequality arises naturally from variation in contribution levels. Under premium membership, distance benefits concentrate among subscribers by construction. More critically, this inequality is **structural and permanent**: a standard agent cannot recover their relative position through contribution alone, because μ is not earned. In the closed economy, a low-scoring agent can always improve by driving. Under premium membership, they cannot. The self-correcting property of the system is removed.

b) Driver supply erodes.: Standard agents observe that high contribution does not produce proportionally better outcomes — premium agents are always prioritized ahead of them regardless of score. The marginal value of driving, already non-monetary, falls further. This erodes voluntary driver participation for the same structural reason as purchasable points: the link between contribution and benefit is severed.

To see this formally, consider the altruism-based reward in Equation 6. The altruism gain term Δs_i^{t+1} is the driver's primary non-monetary incentive. If the score s_i^{t+1} it produces translates into worse matching outcomes than a premium subscription would, the rational agent stops driving and subscribes instead. The volunteer driver pool collapses from the top down: the most mobile agents, exactly those the system most needs as drivers are the most likely to afford a premium subscription and exit the driver pool.

D. The Closed Economy as an Invariant

Both failure modes share the same structure. Each introduces an external resource (money) that substitutes for the internal resource (contribution) used to allocate rights and rewards. Once substitution is possible, s_i^t loses its signal value, and the behavioral incentives (reciprocity, voluntary driving, self-correcting fairness) the closed economy was designed to produce unfold.

This is a specific instance of Goodhart's Law: *when a measure becomes a target, it ceases to be a good measure*. The altruism score functions as a reliable measure of community contribution precisely because it cannot be targeted by financial means.

ORACLE therefore enforces the following invariant across all components of the model:

$$\lambda_i^t = 0 \quad \forall a_i \in A, \quad \forall t \in [1, T] \quad (15)$$

No external injection of altruism points is permitted. Membership tiers, promotional credits, and referral bonuses are all excluded by Equation (D), even when they might appear beneficial for user recruitment. The only path to a high altruism score is driving. The only consequence of a low altruism score is being assigned to drive.

This circularity is not a limitation. It is the mechanism by which the community sustains itself.

E. Connection to System Stability

The equilibrium constraint in Equation (6) states:

$$\frac{|D_t|}{|R_t|} \in [L, H] \quad \text{with } L > 1 \quad (16)$$

This is verified empirically in Section 5.1 via 99% confidence intervals on the time series data. The invariant in Equation (D) is the *mechanism* that makes this empirical result possible. If we remove it through either purchasable points or premium membership, there is no longer any guarantee that the driver supply is self-replenishing. The equilibrium in Equation 16 ceases to hold, and the confidence intervals in Table VI become meaningless.

The closed economy is therefore not merely a design choice about fairness. It is a **precondition for the system's measurable stability properties**.

TABLE VI: 99% CONFIDENCE INTERVALS FOR THE DRIVER-RIDER RATIO UNDER DIFFERENT AGENT DISTRIBUTIONS.

N	Distribution	Mean \pm SD	CV	CI _{low}	CI _{high}
100	Gaussian + B/D	1.14 \pm 0.25	0.21	1.07	1.20
	Gaussian, fixed	1.21 \pm 0.21	0.17	1.16	1.27
	Uniform + B/D	1.13 \pm 0.26	0.23	1.06	1.20
	Uniform, fixed	1.18 \pm 0.20	0.17	1.13	1.23
150	Gaussian + B/D	1.14 \pm 0.16	0.14	1.10	1.18
	Gaussian, fixed	1.22 \pm 0.17	0.14	1.17	1.26
	Uniform + B/D	1.13 \pm 0.17	0.15	1.09	1.18
	Uniform, fixed	1.22 \pm 0.20	0.16	1.16	1.27
200	Gaussian + B/D	1.12 \pm 0.14	0.12	1.08	1.16
	Gaussian, fixed	1.15 \pm 0.14	0.12	1.11	1.19
	Uniform + B/D	1.12 \pm 0.16	0.14	1.07	1.16
	Uniform, fixed	1.15 \pm 0.13	0.11	1.11	1.18

SD: Standard deviation; CV: Coefficient of variation; CI: Confidence interval; B/D: with birth–death dynamics.

Remark 2. Empirically demonstrating these failure modes, simulating a purchasable-points regime and measuring the collapse of the driver-rider ratio via Equation (B), or simulating premium membership and tracking the Gini coefficient trajectory relative to the closed-economy baseline would strengthen this argument further. We leave this as a direction for future work. The theoretical argument is sufficient to motivate the design invariant for the present system.

Appendix C

ORACLE: Algorithm

This section presents the full pseudocode for ORACLE (One-network Actor–Critic for Learning in Cooperative Environments). Algorithm 1 describes the core training step; Algorithm 2 describes the daily role assignment procedure; Algorithm 3 unifies the full multi-day loop across both operational modes.

A. Ego-Conditioned Attention Critic

The critic Q_ϕ evaluates the joint observation–action pair (\mathbf{s}, \mathbf{u}) from the perspective of a specified ego agent i using three separate encoding paths:

- **Query** – ego agent’s observation only, via a state encoder: $e_i^{\text{state}} = f_{\text{state}}(s_i; \phi)$.
- **Keys / Values** – all other agents’ joint (observation, action) pairs via a shared encoder: $e_j^{\text{sa}} = f_{\text{sa}}([s_j; u_j]; \phi)$, $j \neq i$.
- **Ego action** – embedded separately and concatenated with the state embedding and attended features before the final MLP: $e_i^{\text{act}} = f_{\text{act}}(u_i; \phi)$.

Scaled dot-product multi-head attention with temperature T aggregates the other-agent embeddings relative to the ego query. The scalar Q-value is:

$$Q_\phi(\mathbf{s}, \mathbf{u} \mid \text{ego}=i) = \text{MLP}_\phi\left([e_i^{\text{state}}; \text{MHA}_\phi(e_i^{\text{state}}, \{e_j^{\text{sa}}\}_{j \neq i}; T); e_i^{\text{act}}]\right) \quad (17)$$

A *single* weight set ϕ serves all N agent perspectives. Agent identity is conveyed structurally via the ego index, not through learned embeddings, making the parameter count $O(1)$ in N and enabling zero-shot generalisation to unseen population sizes.

B. Deployment and Continual Adaptation

In deployment, π_θ acts as a *recommendation policy*: it proposes a greedy action to each driver, but the human driver decides whether to follow the suggestion. Drivers who deviate from the recommendation—picking a different rider, delaying, or ignoring the suggestion entirely—generate *off-policy transitions* that the trained policy would never

produce on its own. These transitions are stored in \mathcal{D} alongside compliant ones. PER automatically up-weights high-TD-error transitions, which predominantly arise from human deviations, focusing adaptation on exactly those states where the policy is most surprised by real human behavior. This human-in-the-loop mechanism provides genuine off-policy experience beyond the greedy frontier, enabling policy improvement under real-world distribution shift without any engineered exploration that could harm service quality.

Algorithm 1 ORACLE – Core Training Step

```

1: Require: Learning rates  $\alpha_\pi, \alpha_Q$ , discount  $\gamma$ , soft-update rate  $\tau$ , regularisation coefficient  $\lambda$ , exploration strategy  $\mathcal{E} \in \{\epsilon\text{-greedy, TAGS, GST}\}$ 
2: Initialise: Shared actor  $\pi_\theta$ , shared ego-conditioned attention critic  $Q_\phi$ 
3:   Target networks  $\pi_{\theta'} \leftarrow \pi_\theta, Q_{\phi'} \leftarrow Q_\phi$ 
4:   Prioritised replay buffer  $\mathcal{D}$  with parameters  $(\alpha_{\mathcal{D}}, \beta_{\mathcal{D}})$ 
5: repeat
6:   Observe joint state  $\mathbf{s} = (s_1, \dots, s_N)$  and masks  $\mathbf{m} = (\mathbf{m}_1, \dots, \mathbf{m}_N)$ 
7:   for each agent  $i = 1, \dots, N$  do
8:      $\ell_i \leftarrow \pi_\theta(s_i) \odot \mathbf{m}_i$  {Masked logits}
9:      $u_i \leftarrow \mathcal{E}(\ell_i)$  {Action via exploration strategy}
10:  Execute  $\mathbf{u}$ ; observe  $\mathbf{r}, \mathbf{s}', \mathbf{m}'$ 
11:  Store  $(\mathbf{s}, \mathbf{u}, \mathbf{r}, \mathbf{s}', \mathbf{m}, \mathbf{m}')$  in  $\mathcal{D}$ 
12:  if  $|\mathcal{D}| \geq B$  and end of episode then
13:    Sample prioritised mini-batch  $\mathcal{B} = \{(\mathbf{s}^{(k)}, \mathbf{u}^{(k)}, \mathbf{r}^{(k)}, \mathbf{s}'^{(k)}, \mathbf{w}^{(k)})\}$  from  $\mathcal{D}$ 
14:    {— Critic update (all ego perspectives) —}
15:     $\hat{u}'_j \leftarrow \text{softmax}(\pi_{\theta'}(s'_j) \odot \mathbf{m}'_j), \forall j$ 
16:    for ego  $i = 1, \dots, N$  do
17:       $y_i \leftarrow r_i + \gamma(1 - \text{done}) Q_{\phi'}(\mathbf{s}', \hat{\mathbf{u}}' \mid \text{ego}=i)$ 
18:       $\delta_i \leftarrow Q_\phi(\mathbf{s}, \mathbf{u} \mid \text{ego}=i) - y_i$ 
19:       $\mathcal{L}_Q \leftarrow \frac{1}{N} \sum_{i=1}^N \mathbb{E}_{\mathcal{B}}[w \cdot \delta_i^2]$ 
20:       $\phi \leftarrow \phi - \alpha_Q \nabla_\phi \mathcal{L}_Q$ 
21:      {— Actor update (shared policy, all perspectives) —}
22:       $\tilde{u}_j \leftarrow \mathcal{E}_\theta(s_j, \mathbf{m}_j), \forall j$ 
23:       $\mathcal{L}_\pi \leftarrow -\frac{1}{N} \sum_{i=1}^N \mathbb{E}_{\mathcal{B}}[w \cdot Q_\phi(\mathbf{s}, \tilde{\mathbf{u}} \mid \text{ego}=i)] + \lambda \|\theta\|_2^2$ 
24:       $\theta \leftarrow \theta - \alpha_\pi \nabla_\theta \mathcal{L}_\pi$ 
25:      {— Target network soft update —}
26:       $\theta' \leftarrow \tau\theta + (1 - \tau)\theta'; \phi' \leftarrow \tau\phi + (1 - \tau)\phi'$ 
27:      Update  $\mathcal{D}$  priorities:  $\frac{1}{N} \sum_i |\delta_i|$ 
28:    Anneal  $\mathcal{E}, \alpha_{\mathcal{D}}, \beta_{\mathcal{D}}$ , and learning rates
29:  until convergence
    
```

Algorithm 2 Daily Role Assignment

```

1: Input: Active agents  $\mathcal{A}_{\text{active}}$ , altruism scores  $\{s_i^d\}_{i \in \mathcal{A}_{\text{active}}}$ 
2: Output: Role map  $\mathbf{M}_i \in \{\text{driver, rider}\}, \forall i$ 
3:  $s_{\text{max}}^d \leftarrow \max_i s_i^d$ 
4: for each agent  $i \in \mathcal{A}_{\text{active}}$  do
5:   if  $s_i^d \leq 0.2$  then
6:      $\mathbf{M}_i \leftarrow \text{driver}$  {Low altruism  $\Rightarrow$  driver}
7:   else
8:     Draw  $v_1 \sim \mathcal{U}(0, 1)$ 
9:     if  $v_1 < 0.1$  then
10:       $\mathbf{M}_i \leftarrow \text{random}(\text{driver, rider})$  {Role diversification}
11:   else
12:      $p_{\text{rider}} \leftarrow s_i^d / s_{\text{max}}^d$ 
13:     Draw  $v_2 \sim \mathcal{U}(0, 1)$ 
14:      $\mathbf{M}_i \leftarrow \begin{cases} \text{rider}, & v_2 < p_{\text{rider}} \\ \text{driver}, & \text{otherwise} \end{cases}$ 
15: return  $\mathbf{M}$ 
    
```

Algorithm 3 Multi-Day Altruistic Ride-Sharing (ARS)

```

1: Require: Days  $D$ , ORACLE networks  $(\pi_\theta, Q_\phi)$ , mode  $\in \{\text{TRAIN}, \text{DEPLOY+ADAPT}\}$ , replay buffer  $\mathcal{D}$ , batch size  $B$ 
2: If train: exploration strategy  $\mathcal{E}$ , episodes per day  $E$ 
3: Initialise  $\mathcal{A}$  with altruism  $\{s_i^0\}_{i \in \mathcal{A}}$ 
4: for each day  $d = 1, \dots, D$  do
5:    $\mathcal{A}_{\text{active}} \leftarrow \text{UPDATEPOPULATION}(\mathcal{A}, d)$  {Birth / dropout (Eq. 21–23)}
6:    $\mathbf{M} \leftarrow \text{ASSIGNROLES}(\mathcal{A}_{\text{active}}, \{s_i^d\})$  {Alg. 2}
7:   Set  $E_d \leftarrow E$  if mode = TRAIN, else  $E_d \leftarrow 1$  {One real operational day in deployment}
8:   if mode = TRAIN then
9:     Reset  $\mathcal{E}$  to initial temperature /  $\epsilon$ 
10:  for episode  $e = 1, \dots, E_d$  do
11:     $\mathbf{s} \leftarrow \text{RESETENVIRONMENT}(\mathcal{A}_{\text{active}}, \mathbf{M})$ 
12:    while not terminated do
13:      for each active driver  $i \in \mathcal{D}_d$  do
14:        Compute  $\mathbf{m}_i$  from local  $5 \times 5$  perception grid
15:        if mode = TRAIN then
16:           $u_i \leftarrow \mathcal{E}(\pi_\theta(s_i) \odot \mathbf{m}_i)$  {Exploration enabled}
17:        else
18:           $\hat{u}_i \leftarrow \arg \max \text{softmax}(\pi_\theta(s_i) \odot \mathbf{m}_i)$  {Recommend to human driver}
19:           $u_i \leftarrow$  human decision {May differ from  $\hat{u}_i$ ; human deviations provide off-policy experience}
20:        Execute  $\mathbf{u}$ ; observe  $(\mathbf{s}', \mathbf{r})$ 
21:         $s_i^d \leftarrow \text{UPDATEALTRUISM}(s_i^d, u_i, \mathbf{r})$ ,  $\forall i$ 
22:        Store  $(\mathbf{s}, \mathbf{u}, \mathbf{r}, \mathbf{s}', \mathbf{m}, \mathbf{m}')$  in  $\mathcal{D}$ 
23:        Accumulate metrics;  $\mathbf{s} \leftarrow \mathbf{s}'$ 
24:      if  $|\mathcal{D}| \geq B$  then
25:        Run Alg. 1 (lines 12–28) {DEPLOY+ADAPT: off-policy update from human-generated experience; PER up-weights high-error deviation transitions;  $O(1)$  cost in  $N$ }
26:      if mode = TRAIN then
27:        Anneal  $\mathcal{E}$ 
28:       $\{s_i^{d+1}\} \leftarrow \{s_i^d\}$  {Persist altruism across days}
29: Output: Performance metrics, evolved altruism  $\{s_i^D\}$ 
    
```

Appendix D

State, Action, and Reward Details

A. Observation Space

Each agent a_i observes a structured state vector $s_i \in \mathbb{Z}^{28}$ composed of three components:

- **Spatial coordinates:** The (x_i, y_i) position of the agent in the discrete grid environment.
- **Role identifier:** A binary variable $\text{role}_i \in \{0, 1\}$ indicating the agent’s current role (0 = rider, 1 = driver).
- **Local perception field:** A 5×5 observation grid centered on the agent that encodes nearby rider locations and local environmental context. Internally this grid is stored as a flattened vector $\text{grid}_i \in \{-1, 0, \dots, N-1\}^{25}$, where each cell contains the ID of a rider occupying that location, or -1 if the cell is empty.

Together these components form a 28-dimensional observation vector.

B. Action Space

The action space for each agent is discrete:

$$u_i \in \{0, 1, \dots, N\}$$

where $u_i = j$ ($j < N$) corresponds to selecting rider a_j for pickup and $u_i = N$ represents declining all available requests (no-op).

To ensure feasibility, a dynamic action mask \mathbf{m}_i restricts available actions to riders visible in the local 5×5 perception grid, together with the no-op action. This prevents invalid assignments while maintaining computational efficiency.

C. Reward Formulation

The reward received by driver a_i for selecting rider a_j is defined as:

$$r_i = \tanh\left(\alpha_r \cdot d_j(\emptyset) - (1 - \alpha_r) \cdot \Delta d_i(a_j) + \Delta s_i^+\right) \quad (18)$$

where $d_j(\emptyset)$ denotes the standalone trip distance of rider a_j , $\Delta d_i(a_j)$ represents the additional detour incurred by driver a_i to serve that rider, and Δs_i^+ corresponds to the altruism score gained by the driver for completing the ride.

Driver detour distances $\Delta d_i(a_j)$ are computed using Dijkstra’s shortest-path algorithm on the weighted road grid.

Drivers that observe nearby riders but choose the no-op action receive a small baseline reward $\tanh(0.1)$ to discourage persistent inactivity.

D. Hyperparameter Optimization and Exploration Strategy

Training hyperparameters were selected using Bayesian hyperparameter optimization to efficiently explore the parameter space while limiting the number of training runs required. The search procedure evaluated configurations over learning rates, replay buffer parameters, actor and critic network sizes, and exploration schedules. Candidate configurations were sampled using a Bayesian optimization framework that iteratively refined the search distribution based on observed validation performance. The final configuration used in all experiments is summarized in Table VII.

a) Exploration Strategy.: Exploration during training is performed using *Temperature-Annealed Gumbel-Softmax (TAGS)*, which provides a differentiable relaxation of categorical action sampling. Instead of directly sampling discrete actions, the policy samples from a Gumbel-Softmax distribution whose temperature is gradually annealed during training, allowing the distribution to transition from smooth exploratory behavior to near-deterministic action selection.

We also evaluated the Gapped Straight-Through (GST) estimator, in which actions are selected via argmax in the forward pass, while gradients are computed through a deterministic perturbation of the logits in the backward pass. The perturbation enforces a minimum gap between the selected and unselected logits, reducing gradient variance compared to the standard Gumbel-Softmax approach.

While [21] found GST superior in their benchmarks, in our preliminary experiments TAGS provided more stable learning, possibly due to differences in environment complexity or network architecture. Therefore, all reported experiments use TAGS with the temperature annealed from 1.0 to 0.01 over the first 80% of training episodes.

Appendix E Population Dynamics Model

The proposed dynamic population model allows agents to enter (*birth*) and exit (*dropout*) the system over time. Agents occupy one of three states: *active*, *dropped-out*, or *unenrolled*.

A. Dropout Process

Agent dropout probability is governed by individual altruism scores s_i^d (Eq. 19). Low-altruism agents exhibit exponentially higher dropout rates; high-altruism agents maintain stable participation.

$$P_{\text{dropout}}(s_i^d) = \begin{cases} \alpha_{bd} \cdot e^{-\beta_{bd} s_i^d} & \text{if } s_i^d < s_{\text{th}}^d \\ \gamma_{bd} - \delta_{bd} \cdot \frac{s_i^d - s_{\text{th}}^d}{s_{\text{max}}^d - s_{\text{th}}^d} & \text{if } s_i^d \geq s_{\text{th}}^d \end{cases} \quad (19)$$

B. Birth Process

Unenrolled agents may join based on a multi-factor probability model (Eq. 20), where $\rho(d) = (N - N_{\text{never}}(d))/N$ is the community adoption rate.

TABLE VII: SIMULATION AND ORACLE HYPERPARAMETERS

Parameter	Symbol	Value
<i>Environment</i>		
Grid size	$W \times H$	15×15 cells (3.6×4.2 km)
Agent population	N	{100, 150, 200}
Perception radius	—	5×5 grid
Vehicle capacity	l_i	4 passengers
Altruism score range	s_i^d	[0, 1]
Reward trade-off	α_r	0.4
Altruism scaling (driver)	α_s	0.5
Altruism scaling (rider)	β_s	0.7
No-op reward	—	0.1
<i>ORACLE architecture</i>		
Actor hidden layers	—	256 \rightarrow 512
Critic hidden layers	—	256 \rightarrow 512
Attention embedding dim	—	128
Number of attention heads	—	4
Attention temperature	—	1.0
<i>Training</i>		
Critic learning rate	α_Q	1×10^{-4}
Actor learning rate	α_π	1×10^{-5}
Discount factor	γ	0.95
Soft-update rate	τ	0.01
Regularisation	λ	1×10^{-4}
Batch size	B	256
Replay buffer size	$ \mathcal{D} $	50,000
PER $\alpha_{\mathcal{D}}$	—	0.6 (constant)
PER $\beta_{\mathcal{D}}$	—	0.4 \rightarrow 1.0 (linear)
Optimizer	—	AdamW (clip-norm 0.5)
<i>Exploration (Temperature-Annealed Gumbel Softmax)</i>		
Temperature (start \rightarrow end)	—	1.0 \rightarrow 0.01
Decay fraction	—	80% of episodes

$$P_{\text{birth}}(d) = P_{\text{base}}(\rho) \cdot F_{\text{phase}}(\rho) \cdot F_{\text{urgency}}(d) \cdot F_{\text{network}}(N_{\text{active}}) \cdot F_{\text{reputation}}(\bar{s}) \quad (20)$$

- F_{phase} : adoption phase multiplier based on Rogers’ diffusion theory (innovators \rightarrow laggards).
- F_{urgency} : time-sensitive pressure to join ($F_{\text{urgency}} \in [1.0, 3.0]$).
- F_{network} : positive feedback after 30% adoption; congestion effects beyond 85%.
- $F_{\text{reputation}} = 1 + 0.4(\bar{s} - 0.5)$: influence of mean altruism \bar{s} on newcomer interest.

New agents receive initial altruism reflecting behavioural trends across adoption stages: (1) early adopters receive higher scores; (2) network effects boost scores under high participation; (3) scarcity incentives add FOMO bonuses; (4) reputation adjustments reflect recent dropout trends.

C. Population Dynamics

Population counts evolve as:

$$N_{\text{active}}(d+1) = N_{\text{active}}(d) + B(d) - D(d) + R(d) \quad (21)$$

$$N_{\text{never}}(d+1) = N_{\text{never}}(d) - B(d) \quad (22)$$

$$N_{\text{dropout}}(d+1) = N_{\text{dropout}}(d) + D(d) - R(d) \quad (23)$$

where $B(d)$, $D(d)$, and $R(d)$ denote the number of births, dropouts, and reintegrations on day d . Dropped-out agents retain their altruism scores and may rejoin with probability $1 - P_{\text{dropout}}(s_i^d)$.

Appendix F Baseline Implementation Details

A. Particle Swarm Optimisation (PSO)

A swarm of particles is used, where each particle \mathbf{x} represents a feasible rider-to-driver assignment. The fitness function balances rider benefit, driver detour, and altruism:

$$f(\mathbf{x}) = \alpha_r \sum_{j \in \mathcal{R}} d_j(\emptyset) - (1 - \alpha_r) \sum_{i \in \mathcal{D}} (d_i(\phi_i^d | a_j) - d_i(\phi_i^d)) + \beta_{\text{pso}} \sum_{(i,j) \in \mathbf{x}} s_{i,j} \quad (24)$$

The swarm is initialised using a rider-centric geographic strategy. Velocity and position updates follow the standard PSO equations:

$$\mathbf{v}_i^{t+1} = w \mathbf{v}_i^t + c_1 r_1 (\mathbf{p}_i - \mathbf{x}_i^t) + c_2 r_2 (\mathbf{g} - \mathbf{x}_i^t) \quad (25)$$

$$\mathbf{x}_i^{t+1} = \mathbf{x}_i^t + \mathbf{v}_i^{t+1} \quad (26)$$

where \mathbf{p}_i and \mathbf{g} are the personal and global best-known solutions. A repair mechanism enforces capacity constraints after each update.

Appendix G Performance Metrics

We define the following metrics to evaluate ARS.

1) Total Distance and Carbon Emissions.

$$\text{DIST}_{\text{tot}} = \sum_{d=1}^D \sum_{i=1}^N \text{travel}(a_i, d), \quad \text{CO}_2 = \text{DIST}_{\text{tot}} \times \epsilon_{\text{avg}}$$

where ϵ_{avg} is the average emission factor per unit distance.

2) Detour Factor.

$$\text{DET}_{\text{ratio}}(a_i) = \sum_{d=1}^D \frac{d_i(\phi_i^d)}{d_i(\emptyset)}$$

3) Average Trip Time.

$$\text{TIME}_{\text{avg}}(d) = \frac{1}{|\mathcal{A}_{\text{active}}|} \sum_{a \in \mathcal{A}_{\text{active}}} \text{time}(a, d)$$

4) Vehicle Utilisation.

$$\text{UTIL}_{\text{avg}}(d) = \frac{|\mathcal{D}_d| + \sum_{a_j \in \mathcal{R}_d} \mathbb{I}(a_j \text{ travelling at } d)}{|\mathcal{D}_d|}$$

5) Road Traffic Density.

$$\text{DENSE}(d) = \sum_{c \in \text{Grid}} \mathbb{I}(\text{density}(c) > \rho_{\text{threshold}})$$

$$\text{density}(c) = \mathbb{E}_t \sum_{i=1}^N \mathbb{I}(\text{loc}(a_i, t) = c)$$

6) **Rider Acceptance Rate.**

$$\text{ACCEPT}(d) = \frac{\sum_{a_j \in \mathcal{R}_d} \mathbb{I}(a_j \text{ picked up})}{|\mathcal{R}_d|}$$

7) **Benefit Distribution Analysis.**

- a) *3D Lorenz Surface*: cumulative joint distribution of personal benefit (distance saved) and community contribution (traffic reduction).
- b) *Gini Coefficient*: calculated separately per benefit dimension from the 2D projections.

8) **Reintegration Score.**

$$\text{REINT} = \alpha R_{\text{basic}} + \beta R_{\text{time}} + \gamma R_{\text{quick}} + \delta R_{\text{stable}}$$

$$\begin{aligned} R_{\text{basic}} &= \frac{|\mathcal{R}_{\text{re}}|}{|\mathcal{D}_{\text{out}}|} & R_{\text{time}} &= \frac{1}{|\mathcal{R}_{\text{re}}|} \sum_{r \in \mathcal{R}_{\text{re}}} e^{-\lambda_{\text{re}}(d_r - d_o)} \\ R_{\text{quick}} &= \frac{|\{r \in \mathcal{R}_{\text{re}} : d_r - d_o \leq \tau_{\text{re}}\}|}{|\mathcal{R}_{\text{re}}|} & R_{\text{stable}} &= \frac{|\mathcal{S}|}{|\mathcal{U}|} \end{aligned} \quad (27)$$

where \mathcal{R}_{re} is the set of reintegration events $r = (a_i, d_o, d_r)$, \mathcal{D}_{out} is the set of all dropout events, \mathcal{S} is the set of agents who returned and remained stable, and \mathcal{U} is the set of unique returning agents.

Appendix H Additional Experimental Results

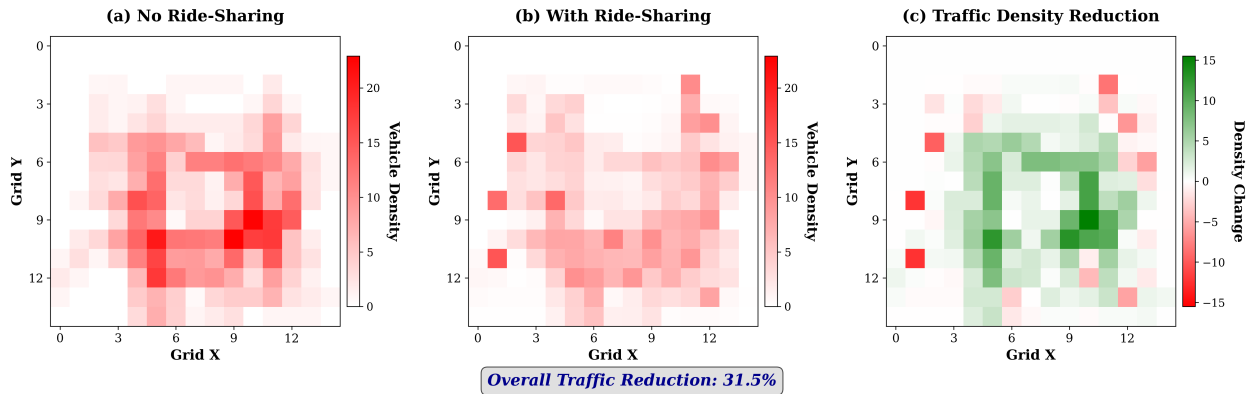
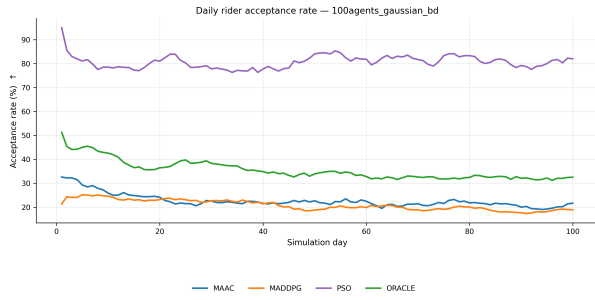
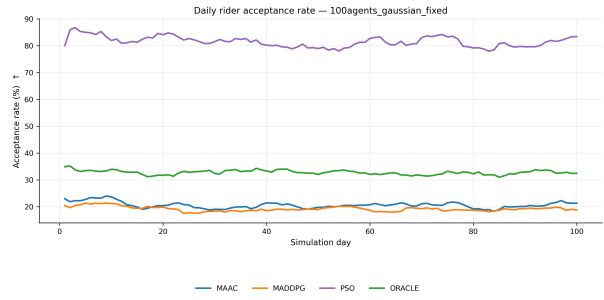


Fig. 12: Comparison of traffic density maps illustrating the reduction in urban congestion achieved by the ARS framework. The figure displays vehicle density for (a) the No Ride-Sharing baseline and (b) the With Ride-Sharing scenario. Subplot (c) visualizes the difference, quantifying a significant overall traffic reduction of 31.5%.

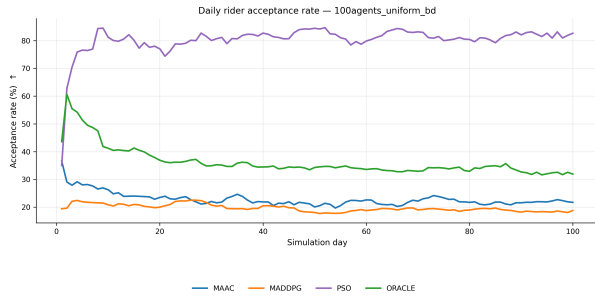
Altruistic Ride Sharing: A Framework for Fair and Sustainable Urban Mobility via Peer-to-Peer Incentives



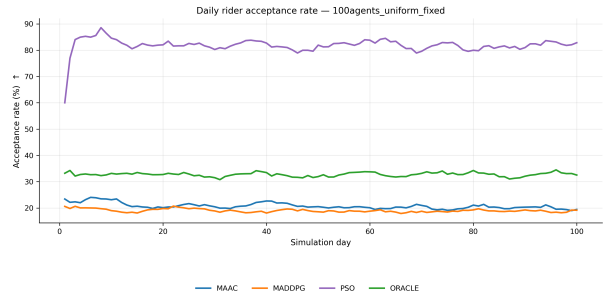
(a) Gaussian allocation; agents may enter and exit (Birth-Death)



(b) Gaussian allocation; no entry and exit of agents

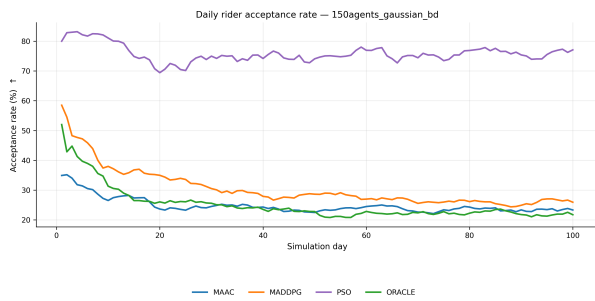


(c) Uniform allocation; agents may enter and exit (Birth-Death)

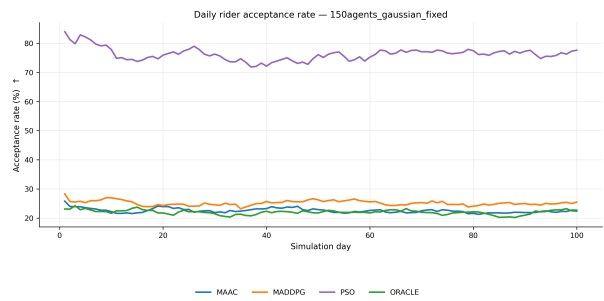


(d) Uniform allocation; no entry and exit of agents

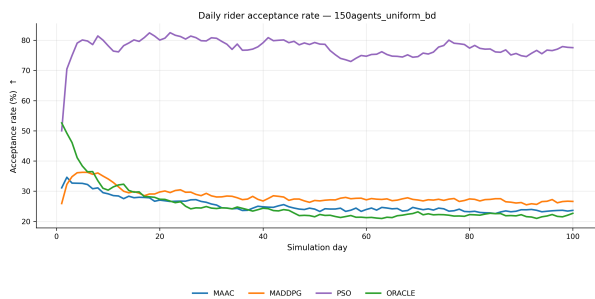
Fig. 13: Daily acceptance rate with 100 agents.



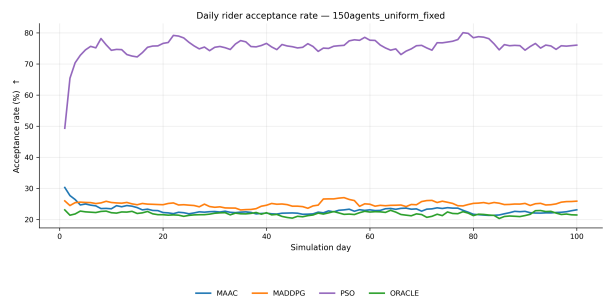
(a) Gaussian allocation; agents may enter and exit (Birth-Death)



(b) Gaussian allocation; no entry and exit of agents

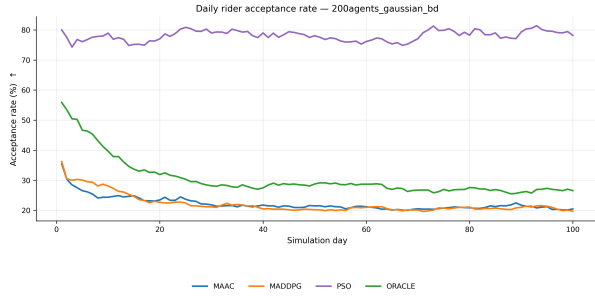


(c) Uniform allocation; agents may enter and exit (Birth-Death)

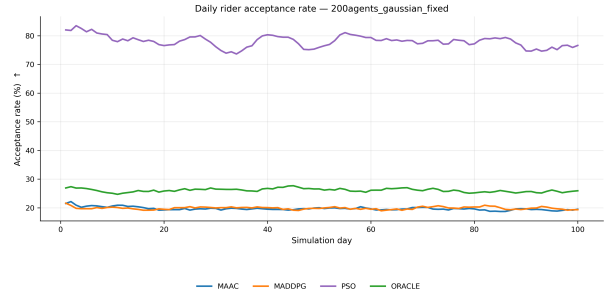


(d) Uniform allocation; no entry and exit of agents

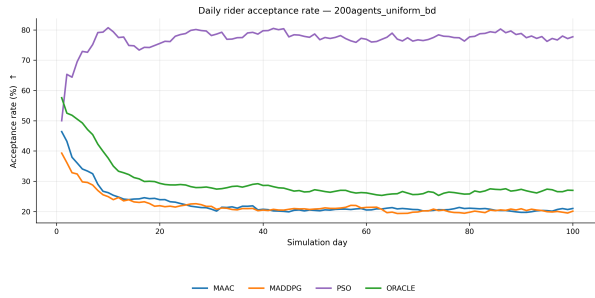
Fig. 14: Daily acceptance rate with 150 agents.



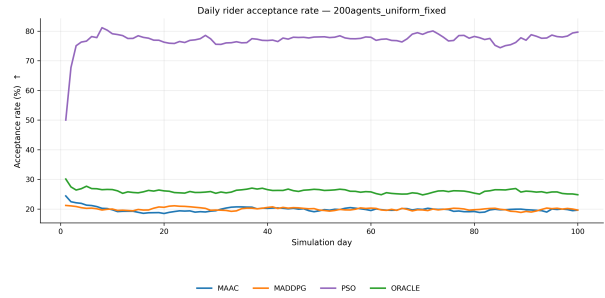
(a) Gaussian allocation; agents may enter and exit (Birth-Death)



(b) Gaussian allocation; no entry and exit of agents

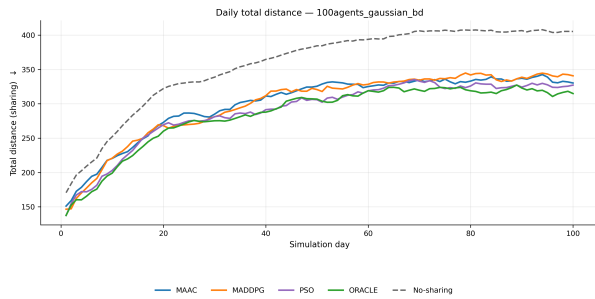


(c) Uniform allocation; agents may enter and exit (Birth-Death)

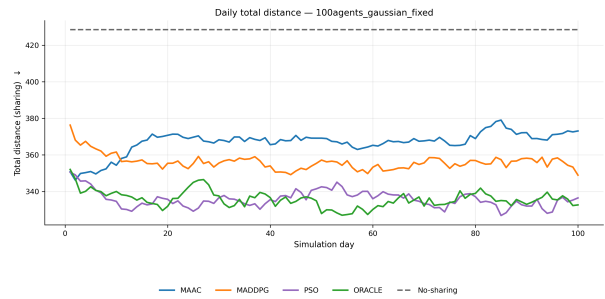


(d) Uniform allocation; no entry and exit of agents

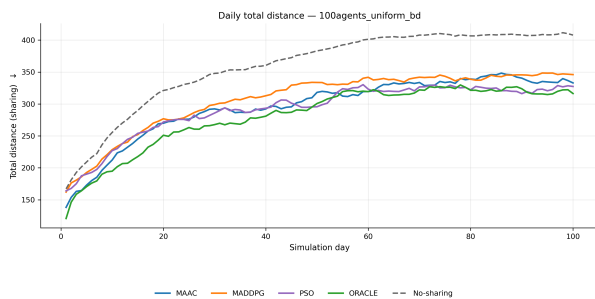
Fig. 15: Daily acceptance rate with 200 agents.



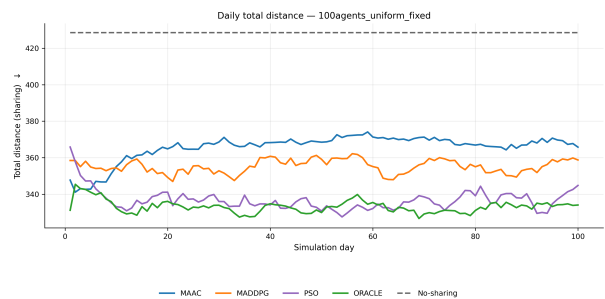
(a) Gaussian allocation; agents may enter and exit (Birth-Death)



(b) Gaussian allocation; no entry and exit of agents

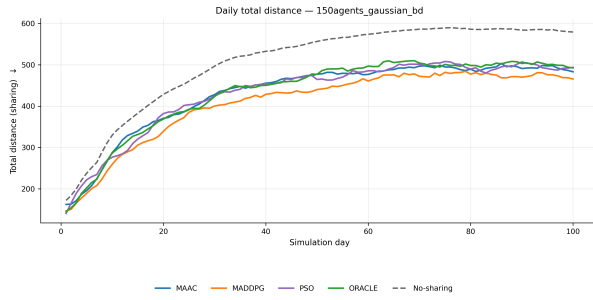


(c) Uniform allocation; agents may enter and exit (Birth-Death)

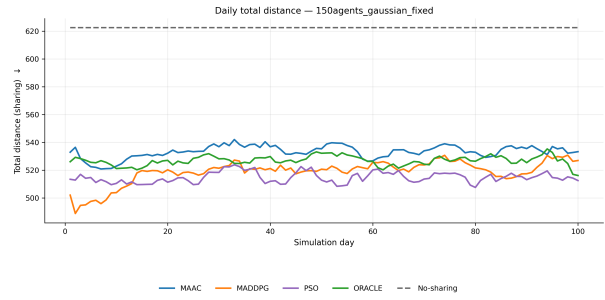


(d) Uniform allocation; no entry and exit of agents

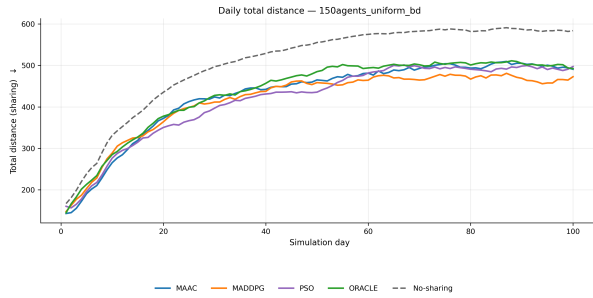
Fig. 16: Daily travel distance with 100 agents.



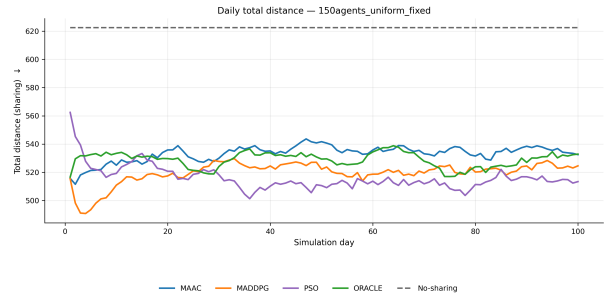
(a) Gaussian allocation; agents may enter and exit (Birth-Death)



(b) Gaussian allocation; no entry and exit of agents

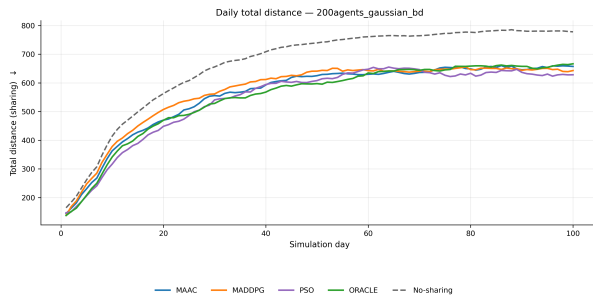


(c) Uniform allocation; agents may enter and exit (Birth-Death)

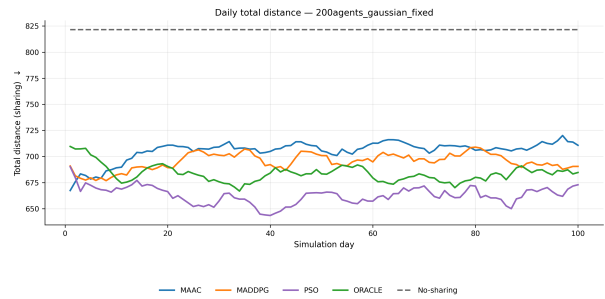


(d) Uniform allocation; no entry and exit of agents

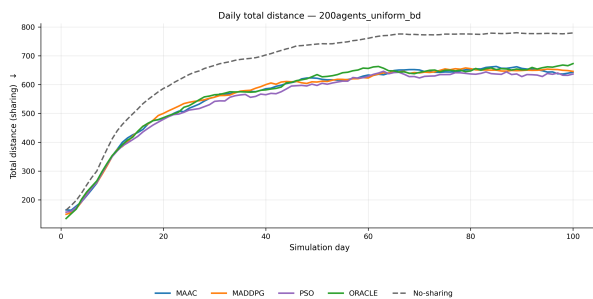
Fig. 17: Daily travel distance with 150 agents.



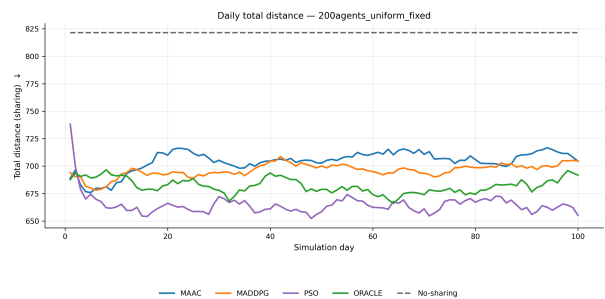
(a) Gaussian allocation; agents may enter and exit (Birth-Death)



(b) Gaussian allocation; no entry and exit of agents



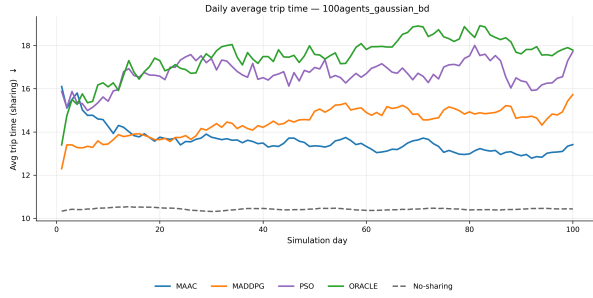
(c) Uniform allocation; agents may enter and exit (Birth-Death)



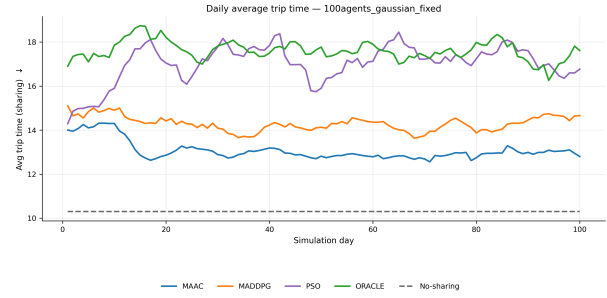
(d) Uniform allocation; no entry and exit of agents

Fig. 18: Daily travel distance with 200 agents.

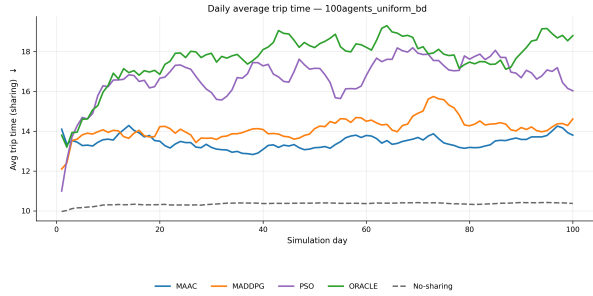
Altruistic Ride Sharing: A Framework for Fair and Sustainable Urban Mobility via Peer-to-Peer Incentives



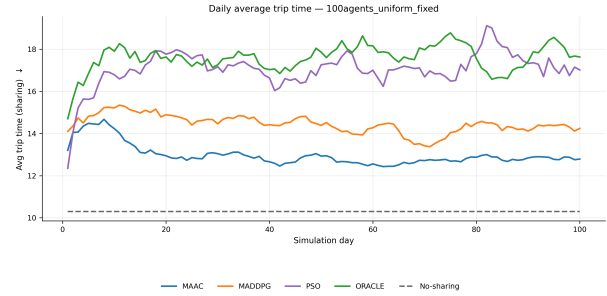
(a) Gaussian allocation; agents may enter and exit (Birth-Death)



(b) Gaussian allocation; no entry and exit of agents

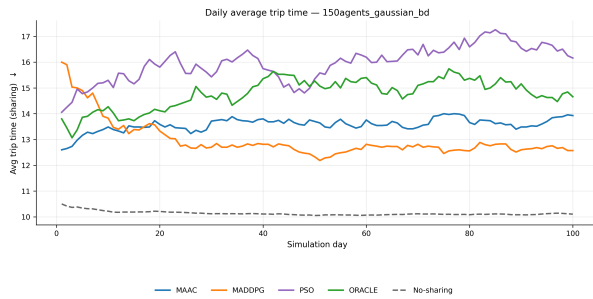


(c) Uniform allocation; agents may enter and exit (Birth-Death)

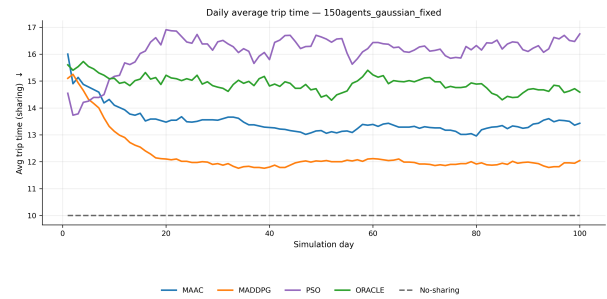


(d) Uniform allocation; no entry and exit of agents

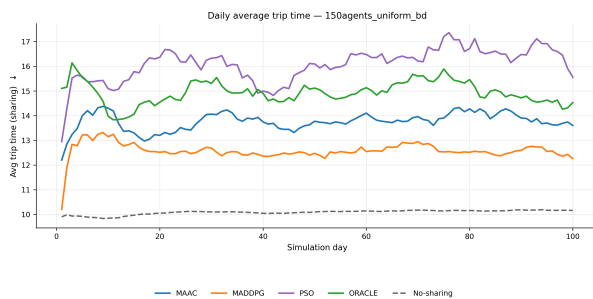
Fig. 19: Daily trip time with 100 agents.



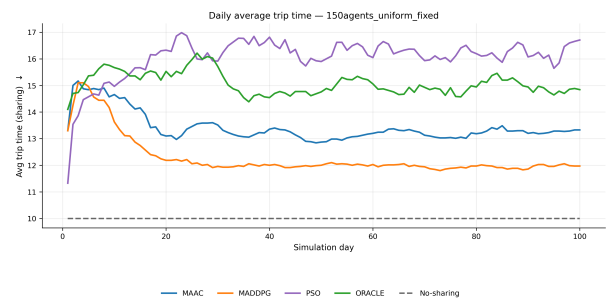
(a) Gaussian allocation; agents may enter and exit (Birth-Death)



(b) Gaussian allocation; no entry and exit of agents



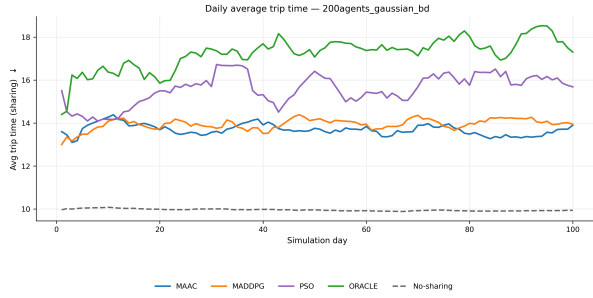
(c) Uniform allocation; agents may enter and exit (Birth-Death)



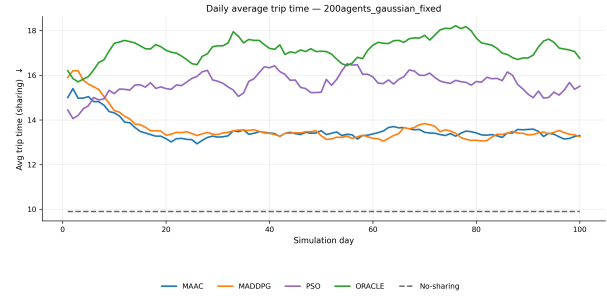
(d) Uniform allocation; no entry and exit of agents

Fig. 20: Daily trip time with 150 agents.

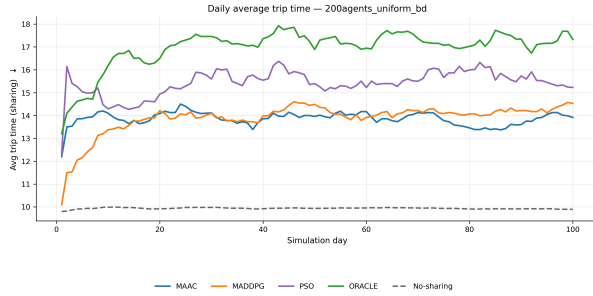
Altruistic Ride Sharing: A Framework for Fair and Sustainable Urban Mobility via Peer-to-Peer Incentives



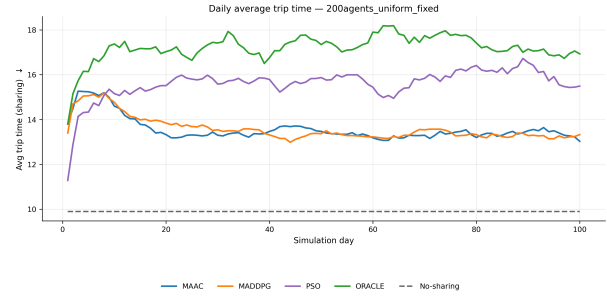
(a) Gaussian allocation; agents may enter and exit (Birth-Death)



(b) Gaussian allocation; no entry and exit of agents

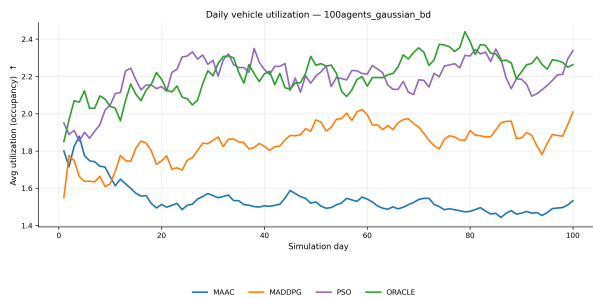


(c) Uniform allocation; agents may enter and exit (Birth-Death)

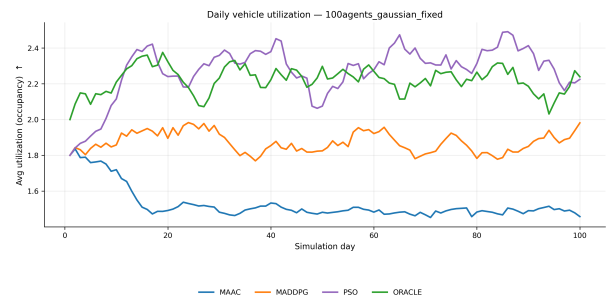


(d) Uniform allocation; no entry and exit of agents

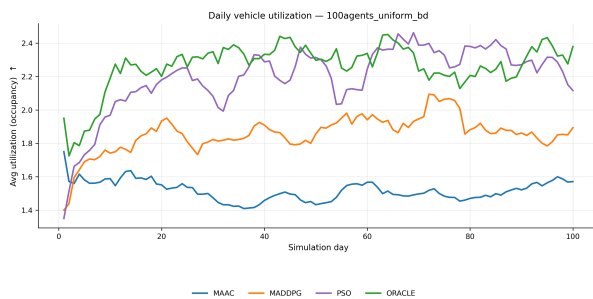
Fig. 21: Daily trip time with 200 agents.



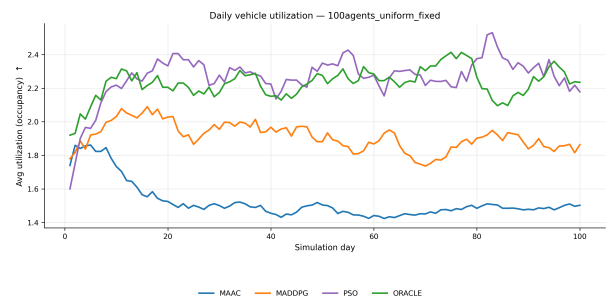
(a) Gaussian allocation; agents may enter and exit (Birth-Death)



(b) Gaussian allocation; no entry and exit of agents

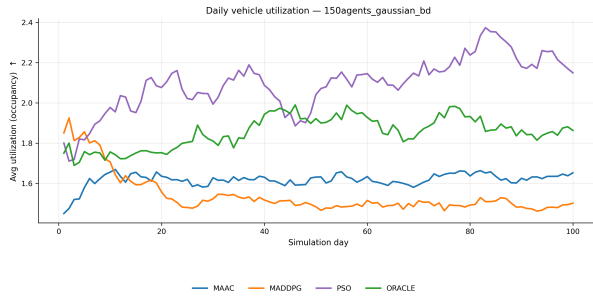


(c) Uniform allocation; agents may enter and exit (Birth-Death)

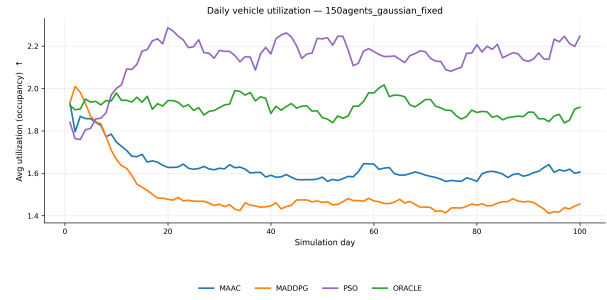


(d) Uniform allocation; no entry and exit of agents

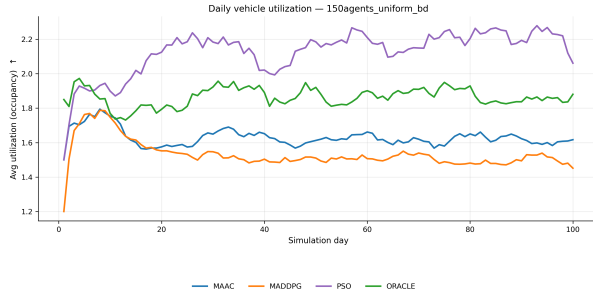
Fig. 22: Daily vehicle utilization with 100 agents.



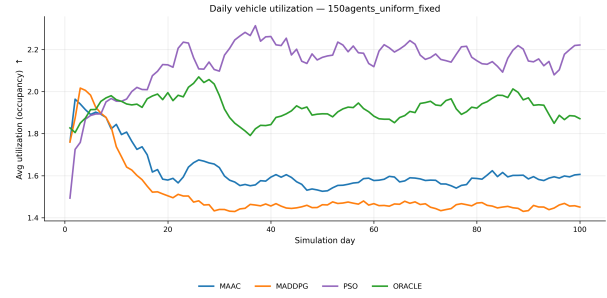
(a) Gaussian allocation; agents may enter and exit (Birth-Death)



(b) Gaussian allocation; no entry and exit of agents

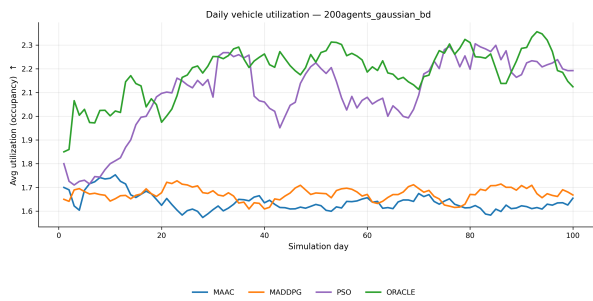


(c) Uniform allocation; agents may enter and exit (Birth-Death)

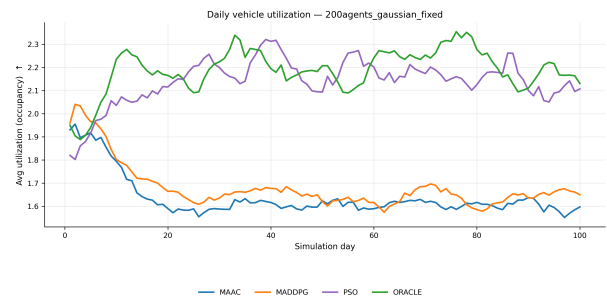


(d) Uniform allocation; no entry and exit of agents

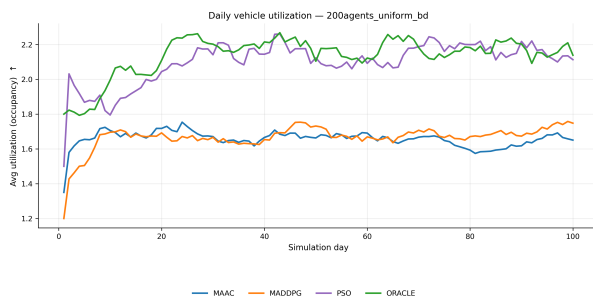
Fig. 23: Daily vehicle utilization with 150 agents.



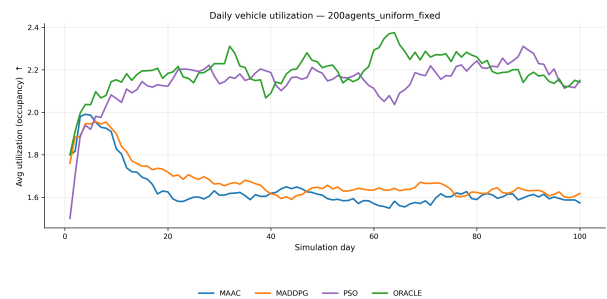
(a) Gaussian allocation; agents may enter and exit (Birth-Death)



(b) Gaussian allocation; no entry and exit of agents



(c) Uniform allocation; agents may enter and exit (Birth-Death)



(d) Uniform allocation; no entry and exit of agents

Fig. 24: Daily vehicle utilization with 200 agents.

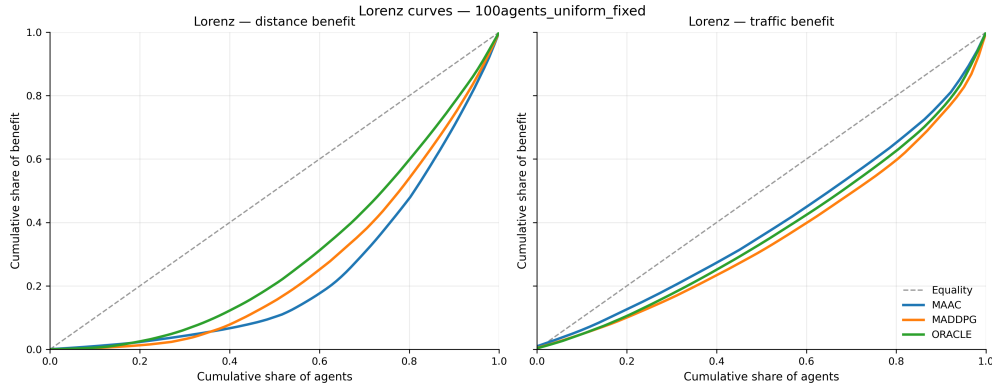


Fig. 25: Lorenz curve overlay illustrating distributional inequality in outcomes for the 100-agent setting with uniform altruism allocation and no entry or exit of agents.

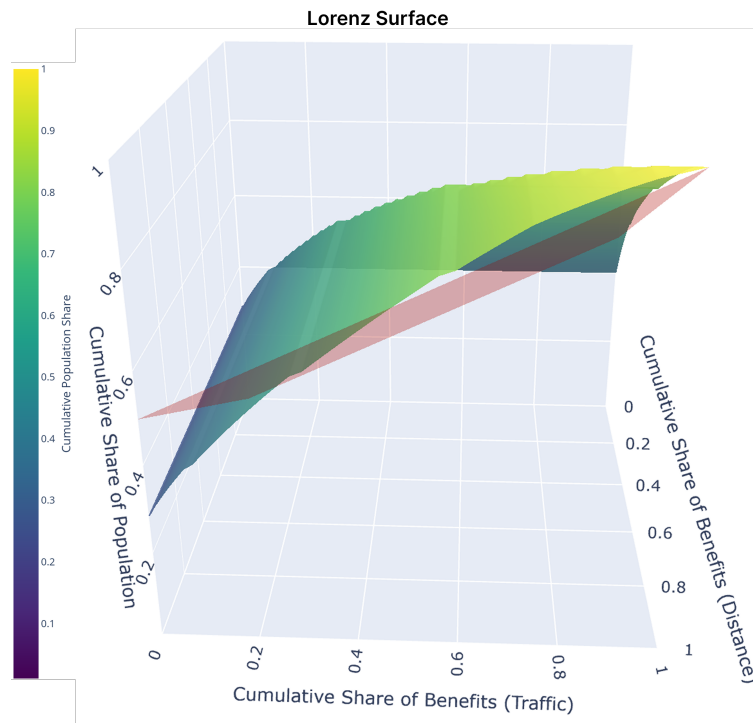


Fig. 26: Three-dimensional Lorenz surface representing joint inequality in cumulative shares of population, distance benefits, and traffic benefits from ride-sharing. The surface deviates from the diagonal plane (perfect equality), highlighting heterogeneity in benefit distribution. Positive distance benefits Gini ≈ 0.471 , indicating moderate inequality in distance savings. Traffic Benefits Gini ≈ 0.235 , indicating relatively more equitable distribution of congestion-related gains. A Granger-causality analysis reveals that past altruism significantly predicts subsequent benefits ($p = 0.0038$ at the system level), providing evidence that heterogeneity in altruism contributes to the observed concentration of benefits.

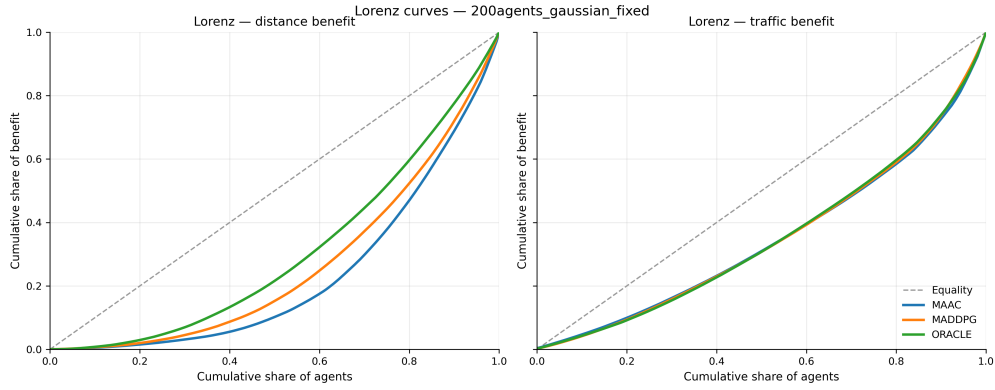


Fig. 27: Lorenz curve overlay illustrating inequality in system outcomes for the 200-agent scenario with Gaussian altruism allocation and no entry or exit of agents.

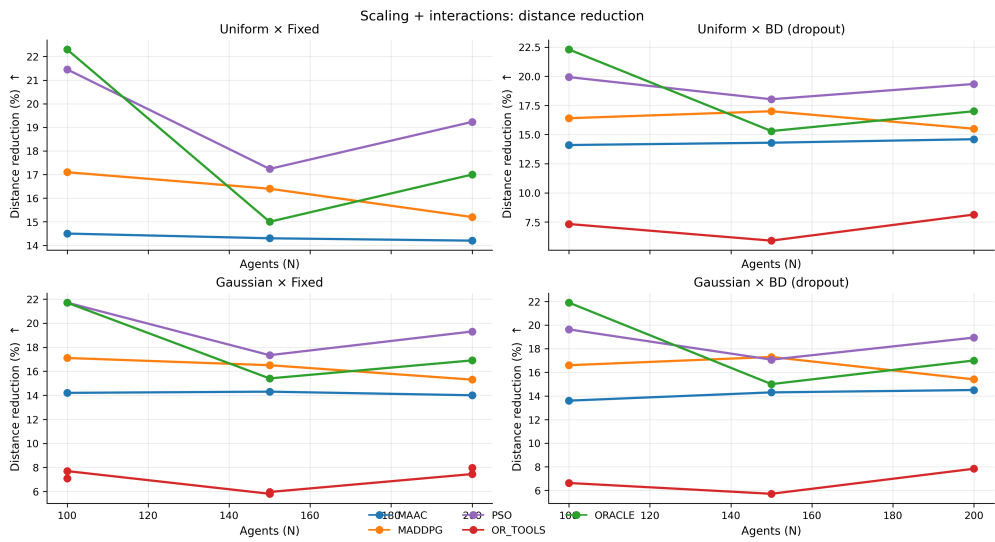


Fig. 28: Interaction analysis showing the relationship between altruism mechanisms and overall distance reduction in the transportation system.

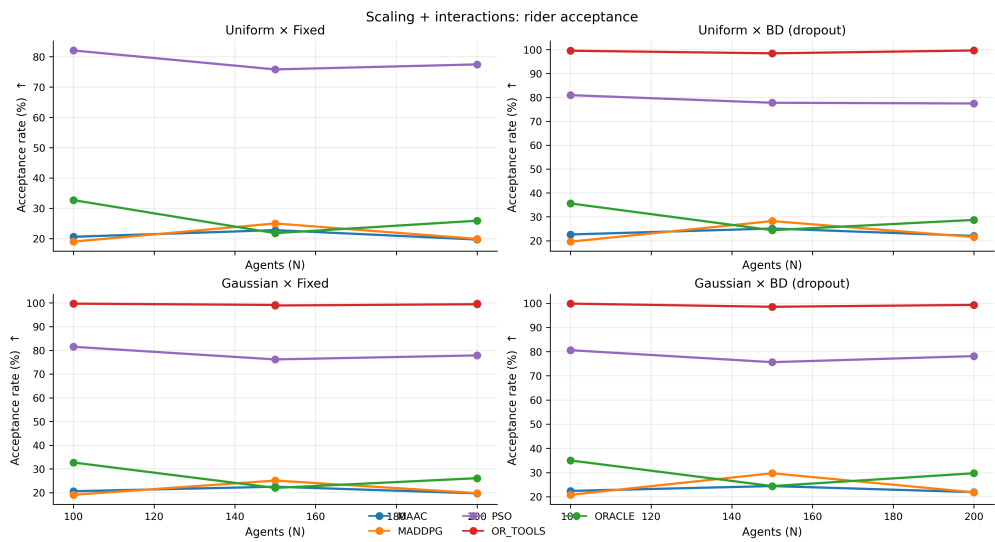


Fig. 29: Interaction effects illustrating how altruism dynamics influence ride acceptance rates across agents.

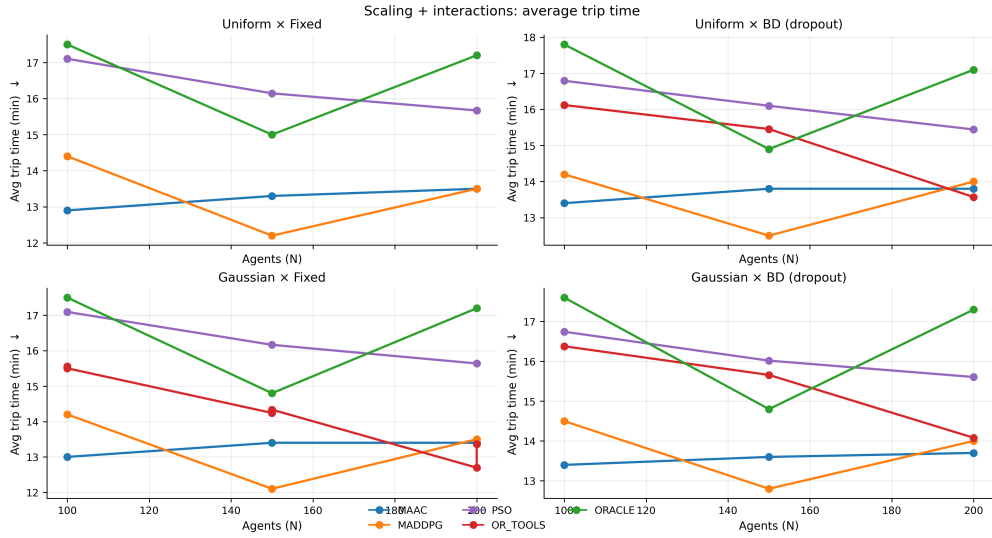


Fig. 30: Interaction effects between system parameters and average trip time outcomes.

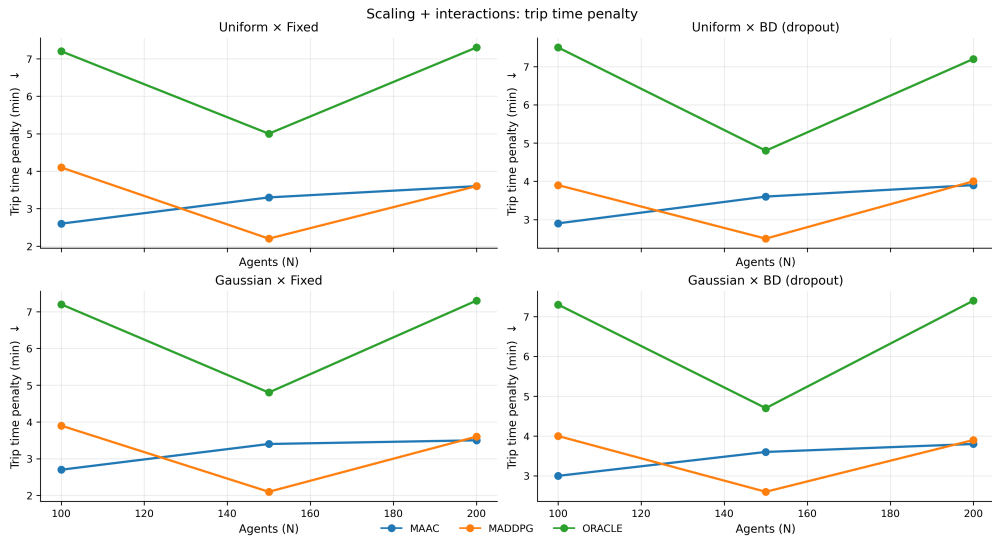


Fig. 31: Interaction analysis showing changes in trip time relative to baseline system configurations.

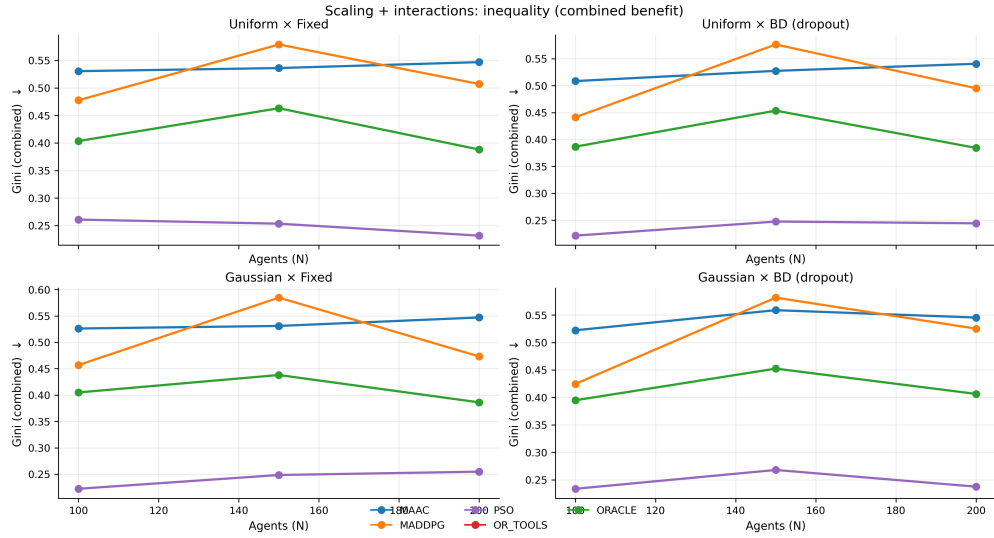


Fig. 32: Interaction effects on the Gini coefficient, measuring inequality in benefits among participating agents.

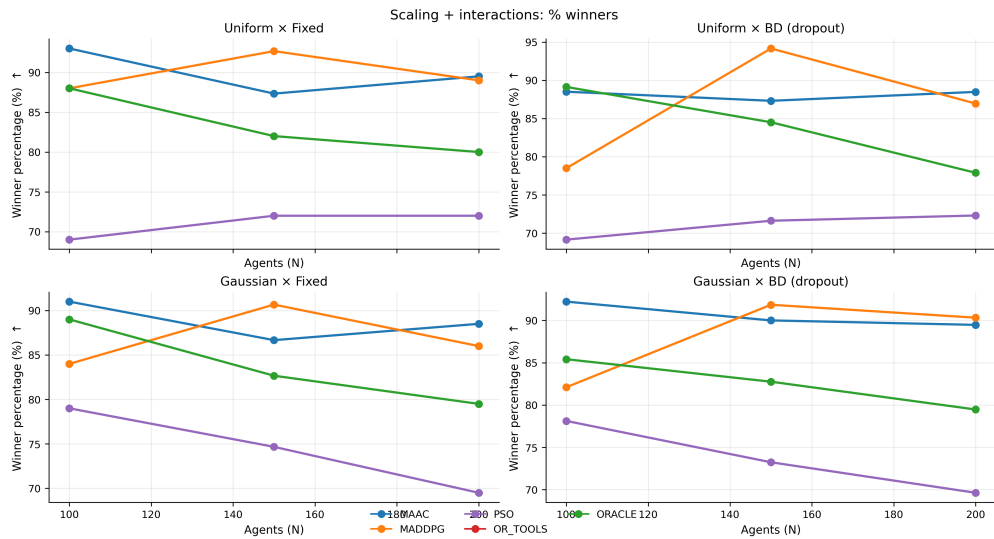
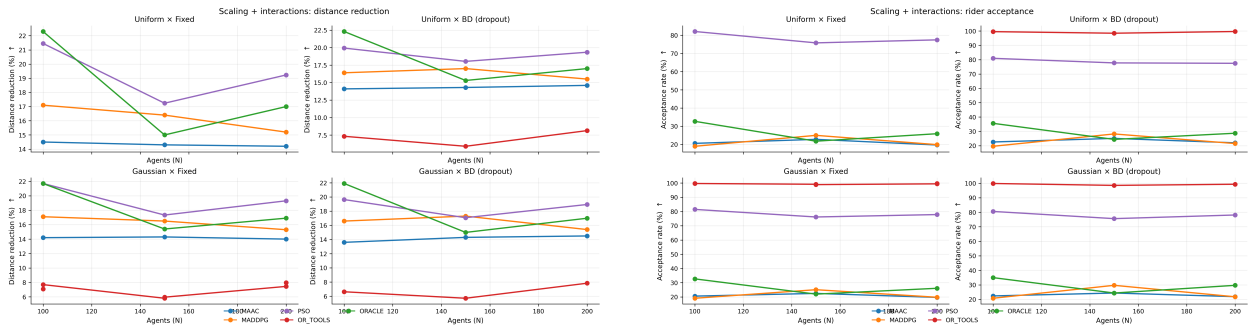


Fig. 33: Analysis of agents benefiting most under different altruism-based allocation mechanisms.



(a) Impact of altruism mechanisms on overall distance reduction.

(b) Impact of altruism dynamics on ride acceptance rates.

Fig. 34: Interaction analyses showing how altruism mechanisms affect key transportation metrics.

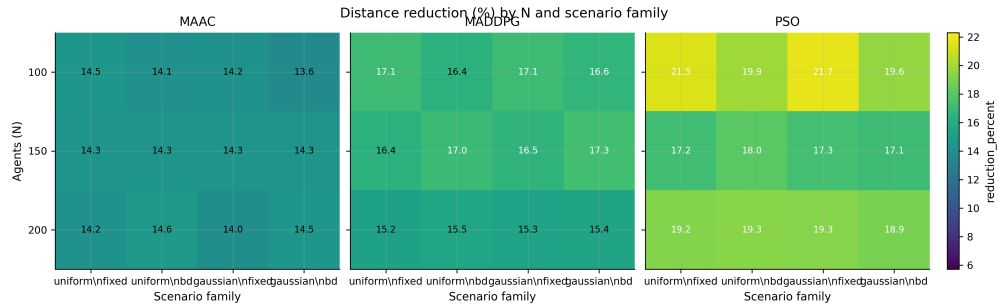


Fig. 35: Heatmap illustrating distance reduction across families of experimental configurations.

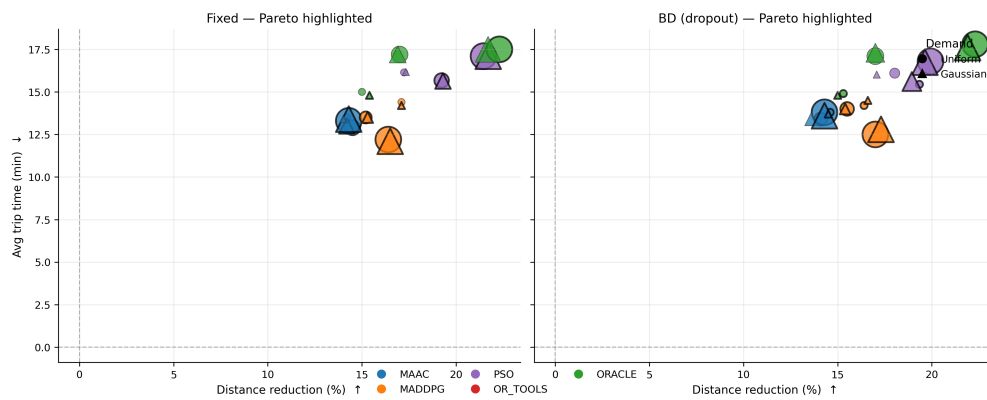
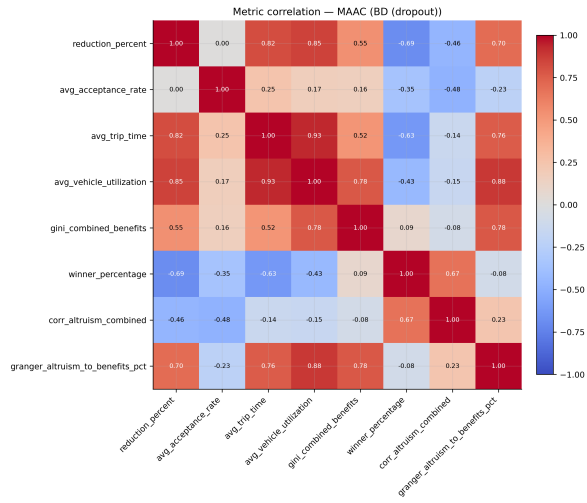
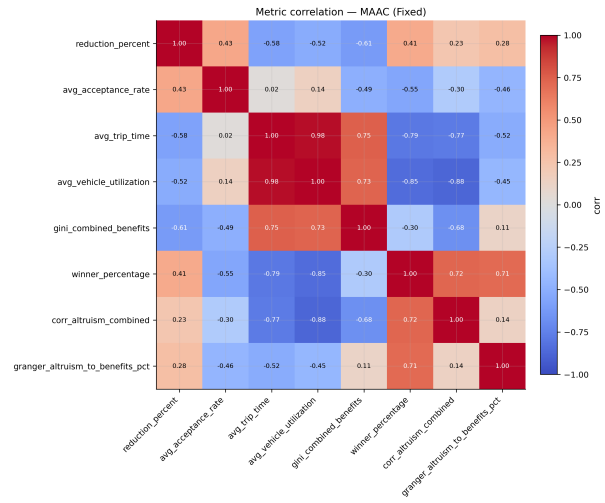


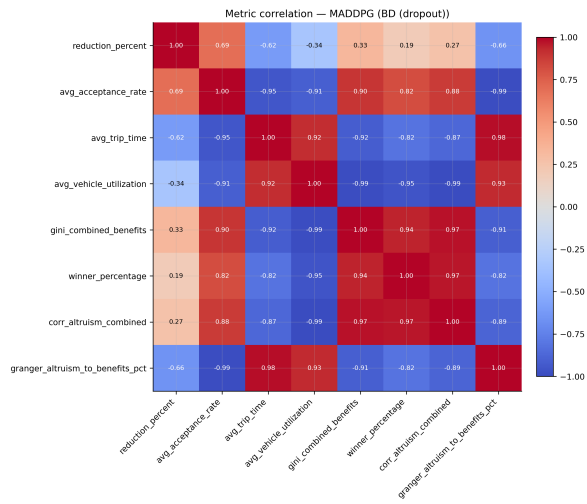
Fig. 36: Pareto frontier illustrating trade-offs between efficiency improvements and equity outcomes across system configurations.



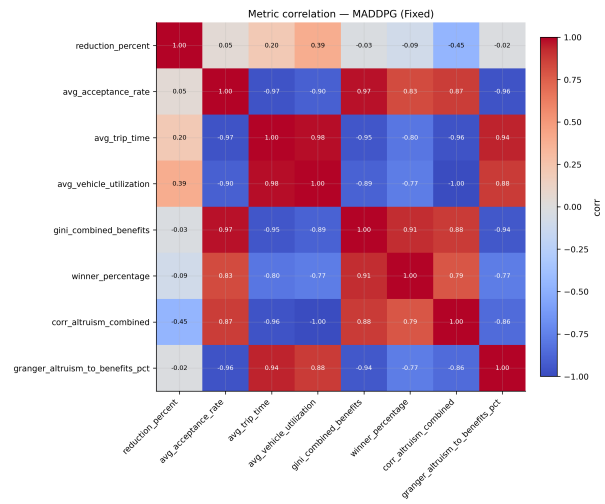
(a) MAAC — agents may enter and exit (Birth–Death)



(b) MAAC — no entry and exit of agents



(c) MADDPG — agents may enter and exit (Birth–Death)



(d) MADDPG — no entry and exit of agents

Fig. 37: Correlation matrices of key system metrics for multi-agent reinforcement learning approaches under different population dynamics.

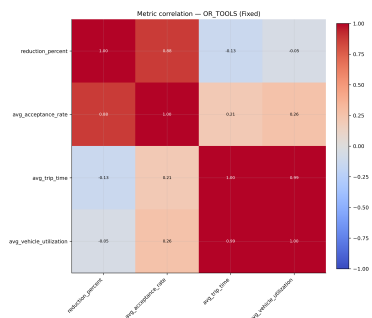
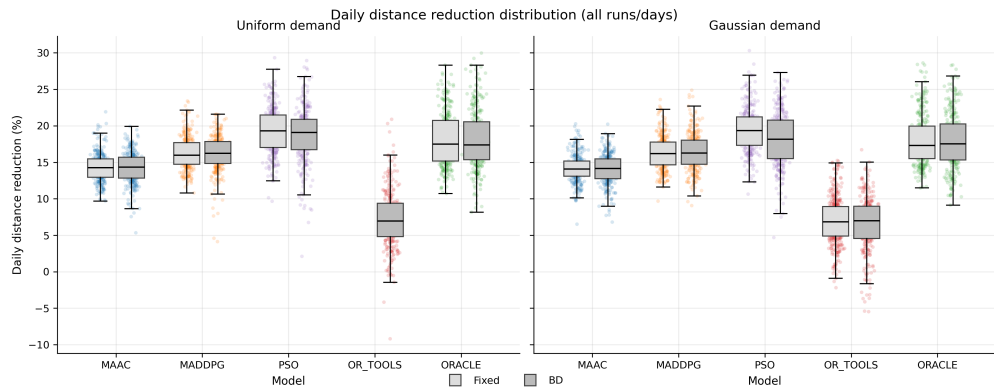
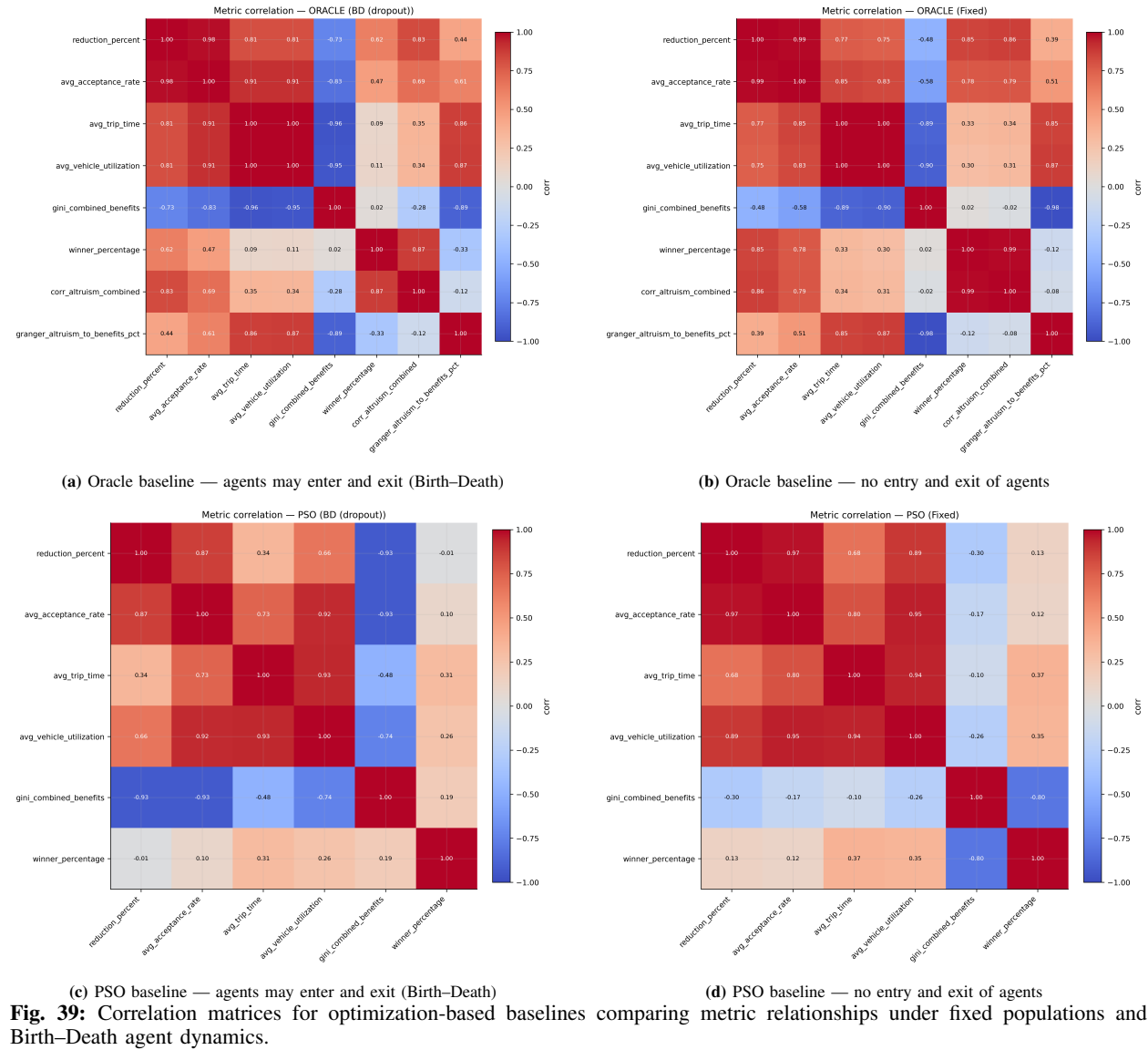


Fig. 38: Correlation matrix of key performance metrics for the OR-Tools baseline with fixed agents.



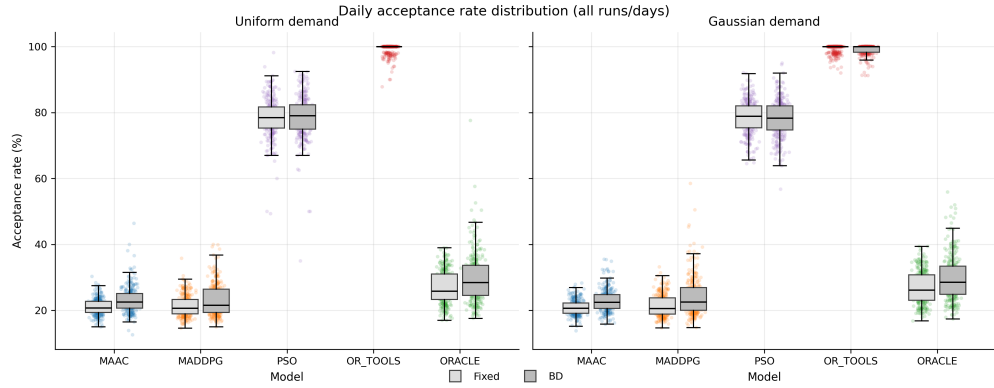


Fig. 41: Distribution of ride acceptance rates across system configurations.

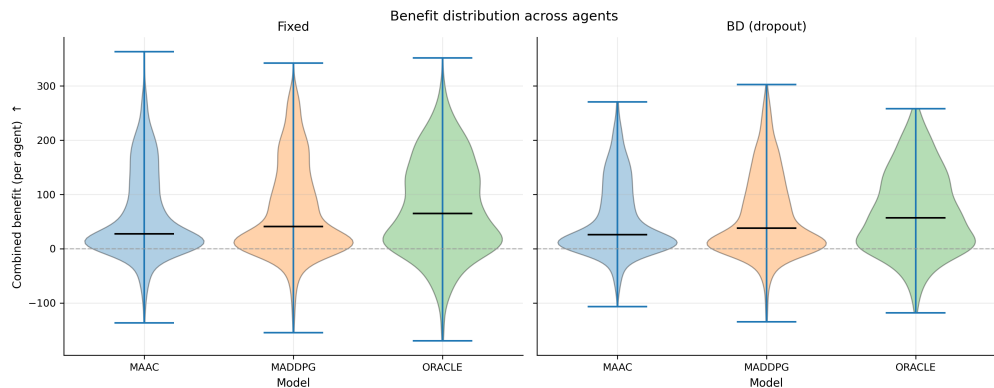


Fig. 42: Violin plot showing distribution of agent-level benefits under different altruism allocation mechanisms.

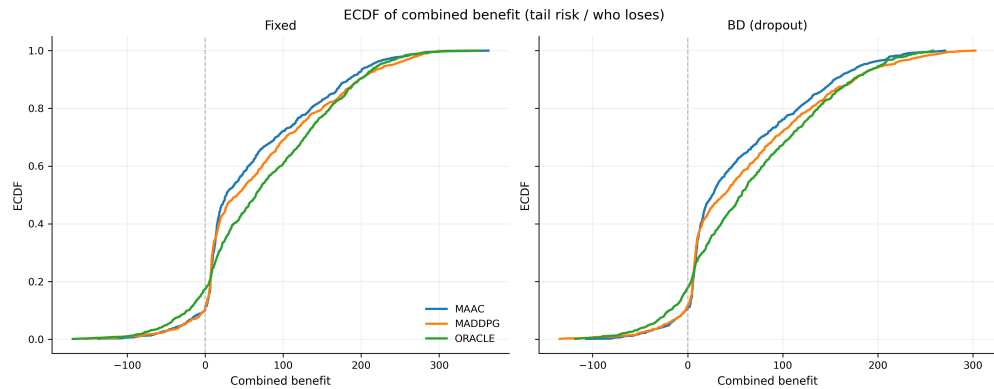


Fig. 43: Empirical cumulative distribution of agent-level benefits across all experimental configurations.

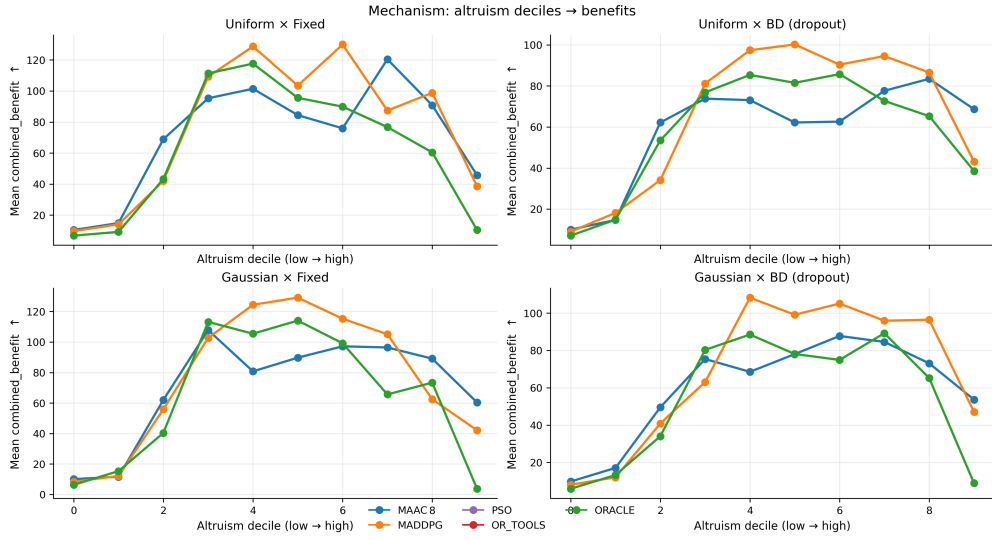


Fig. 44: Benefit outcomes across altruism deciles illustrating how system gains vary with agent altruism levels.

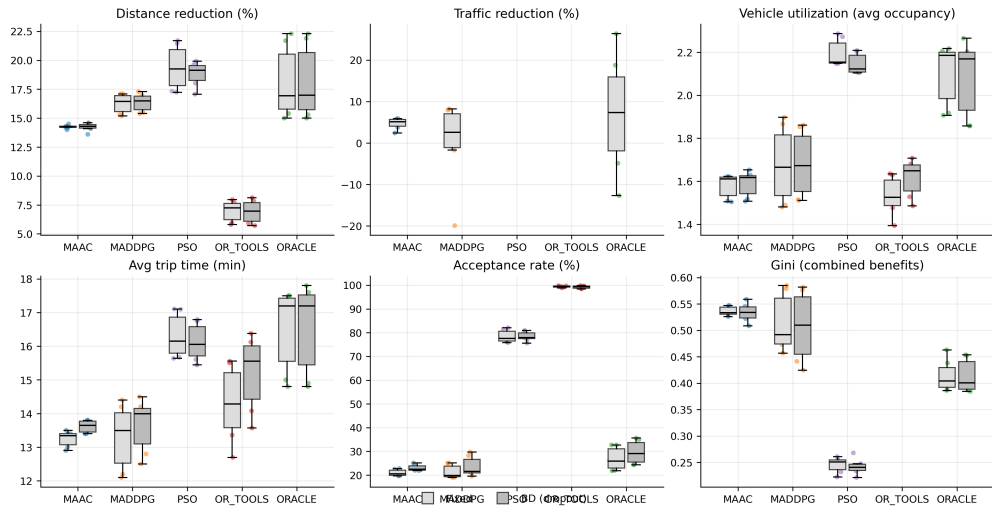


Fig. 45: Boxplots summarizing the distribution of core system performance metrics across all experimental scenarios.

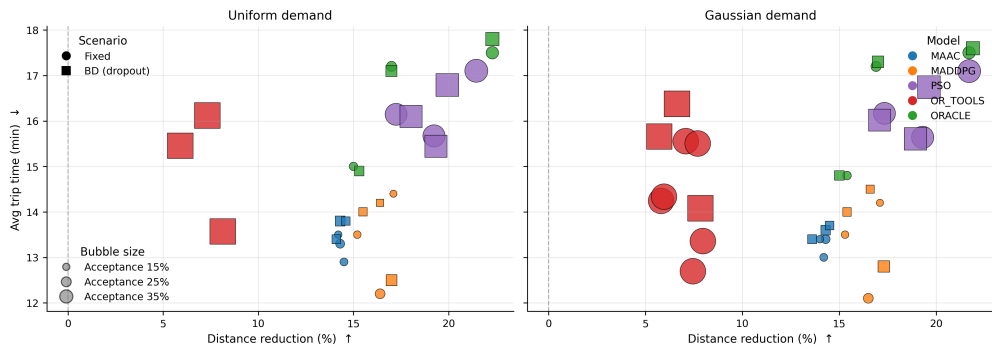


Fig. 46: Trade-off analysis illustrating relationships between efficiency improvements and equity outcomes.

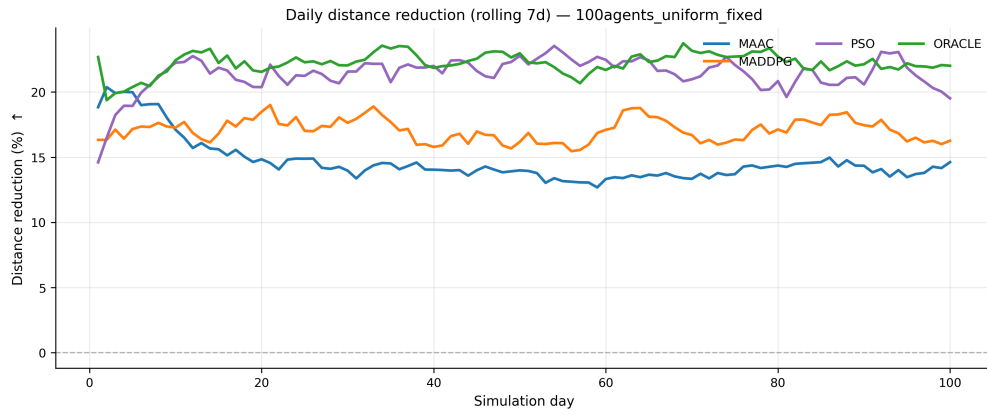


Fig. 47: Daily distance reduction over time for the 100-agent scenario with uniform altruism allocation and no entry or exit of agents.

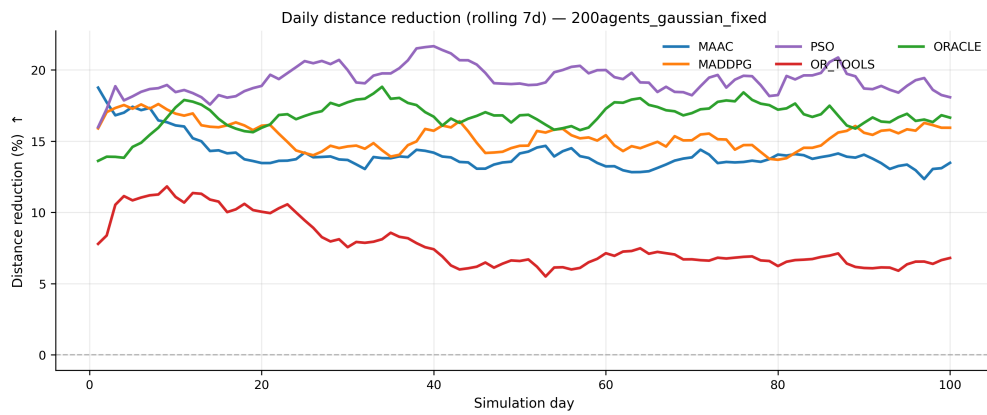


Fig. 48: Daily distance reduction over time for the 200-agent scenario with Gaussian altruism allocation and no entry or exit of agents.